Aerodynamic Parameters for Control Fins

Research and Development Report

Prepared for NARCON 2026

Rev 1.1

Feb 25, 2026

Thomas B Fetter

NAR 15551

C Division

Summary

This paper is the first in a series of papers that will document the author's vertical orientation control project. The vertical orientation control rocket configuration consists of four forward mounted control canards and four rear mounted fins. The canards are rotated to control the pitch, yaw, and roll of the rocket. To design the pitch and roll control systems, a model of the pitch and roll rotational dynamics is needed, and for that, the aerodynamic parameters for the control fins or canards are required.

The derivation of most of the required aerodynamic parameters is documented in James Barrowman's Master's thesis or in the references cited by Barrowman. But there are some necessary pieces that are missing from Barrowman. This paper presents all the aerodynamic parameters for rotated fins or canards needed to design a vertical orientation control system including the pitch and roll forcing and damping moments and all the individual normal force coefficient derivatives and tail-body interference factors that make up the pitch and roll moments, as well as the components of the angle-of-attack of the rotated fins or canards.

Test rocket flight data and NASA wind tunnel test model data are used to verify that the forward mounted canards are not effective for roll control due to the canard downwash interference with the fins, which leads to the vertical orientation rocket's use of a freely rotating fin section, or spin-can. With the spin-can, the flight data from the test rocket using roll control matches the flight simulation using the parameters presented in the paper very closely. The flight data from the rocket using pitch and yaw control also matches the flight simulation using the parameters from this paper. The data and modeling show that the canard downwash has little impact on the pitch aerodynamic parameters.

Table of Contents

1 Introduction

1.1 Objective and Approach

The objective of this paper is to provide all the aerodynamic parameters for control fins that are needed to create the rotational dynamics model for a vertical orientation control system where the fins are rotated to control the yaw, pitch, and roll of the rocket. Those aerodynamic parameters include the roll and pitch forcing and damping normal forces and rotational moments, and all the normalized coefficients and interference factors that are used in calculating the moments, the components of the angle-of-attack of the fins or canards needed for pitch, yaw, and roll control, as well as the correct signs for all the parameters in the defined axis system. Although most of the required parameters and the methodologies for deriving those parameters are covered in Barrowman's Master's thesis[1] or in the papers cited by Barrowman, there are some pieces required for orientation control that are missing from Barrowman.

The approach is to use the methods from the papers cited by Barrowman in conjunction with the analytic tool Mathcad to fill in the missing pieces and provide a comprehensive set of parameters. It is also an objective for this paper to serve as a standalone document so that the reader does not have to refer to multiple papers to understand the derivation and use of the aerodynamic parameters.

This paper is one of a series of papers that will document the author's vertical orientation control project. Figure 1-1 shows the various design tasks needed to design a rocket with a vertical orientation control system, including the modeling work. This paper covers just the first box in red, Aerodynamic Modeling for Control Fins. Future papers will cover the other modeling tasks, including the pitch and roll dynamics modeling, control system design, the servo motor modeling, as well as the implementation of the vertical orientation control system rocket.

The nomenclature used in this paper most closely aligns with Mandell's since this project started as a study of rotational dynamic stability, the topic of Mandell's chapter in *Topics in Advanced Model Rocketry*[2]. The nomenclature is consistent with that used in the aerodynamic and control system models used throughout this vertical orientation control project documentation.

A vertical orientation control system can use steerable fins or canards to control the pitch, yaw, and roll of the rocket. Canards are just a second set of fins, usually smaller than the main fins, that are used as the control surfaces.

---

[1] (Barrowman J. S., The Practical Calculation of the Aerodynamic Characteristics of Slender Finned Vehicles, Master's Thesis, 1967)

[2] (Mandell, Caporaso, & Bengen, 1973)

For model and high power rockets, the control canards are typically located toward the front of the rocket to provide room for the servo motors. The aerodynamic parameters for canards are the same as for fins. This paper generalizes by referring to the control surface a fin and does not make a distinction until Section 4 where a rocket with both fins and canards is considered. If the rocket uses canards to control the orientation of the rocket, then the fin parameters derived in this paper would be applied to the canards. These same parameters can also be used to model the impact of misaligned fins on the pitch and roll of a rocket.

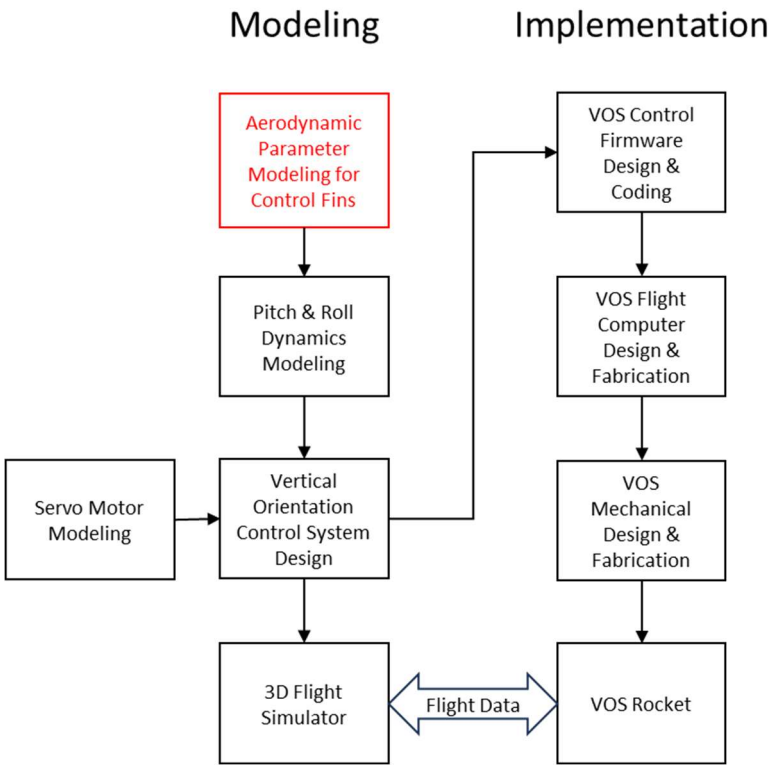

Figure 1-1 Vertical Orientation Control project

1.2 Prior Work

James Barrowman's master's thesis[3] provides a very comprehensive framework for the calculation of the aerodynamic characteristics of fin stabilized rockets including the parameters needed to model the aerodynamics of

[3] (Barrowman J. S., The Practical Calculation of the Aerodynamic Characteristics of Slender Finned Vehicles, Master's Thesis, 1967)

control fins and canards. The aerodynamic parameters include the roll and pitch forcing and damping moments, and all the normal force coefficient derivatives and interference factors that are used in calculating the moments. Figure 1-2 shows an index of the sections of Barrowman's thesis that cover the parameters of interest for control fins and canards.

Parameter	Section/Page
Normal force coefficient derivative – Single Fin	3.11 p. 3
Normal force coefficient derivative – Multiple Fins for Pitch	3.11 p. 4
Normal force coefficient derivative – Multiple Fins for Roll	3.13 p. 11
Tail-Body Interference Factor due to Body Angle-of-attack	3.31 p. 31 NARAM 3 R&D p. 36
Tail-Body Interference Factor Due to Fin Angle	3.33 p. 37
Pitch Damping Moment	3.41 p. 37
Roll Forcing Moment	3.13 p. 11
Roll Damping Moment	3.14 p. 11
Roll Damping Tail-Body Interference	3.42 p. 41
Fin Center of Pressure	3.12 p. 6

Figure 1-2 Fin aerodynamic parameter index for Barrowman's thesis

Barrowman's thesis draws on the work done by a number of other researchers. Although Barrowman's thesis is very comprehensive, these sources provide additional useful details and insights into the modeling of the aerodynamic parameters. Figure 1-3 shows the references Barrowman used, as well as several follow-on works, and the key contribution of each that pertain to the fin aerodynamic parameters.

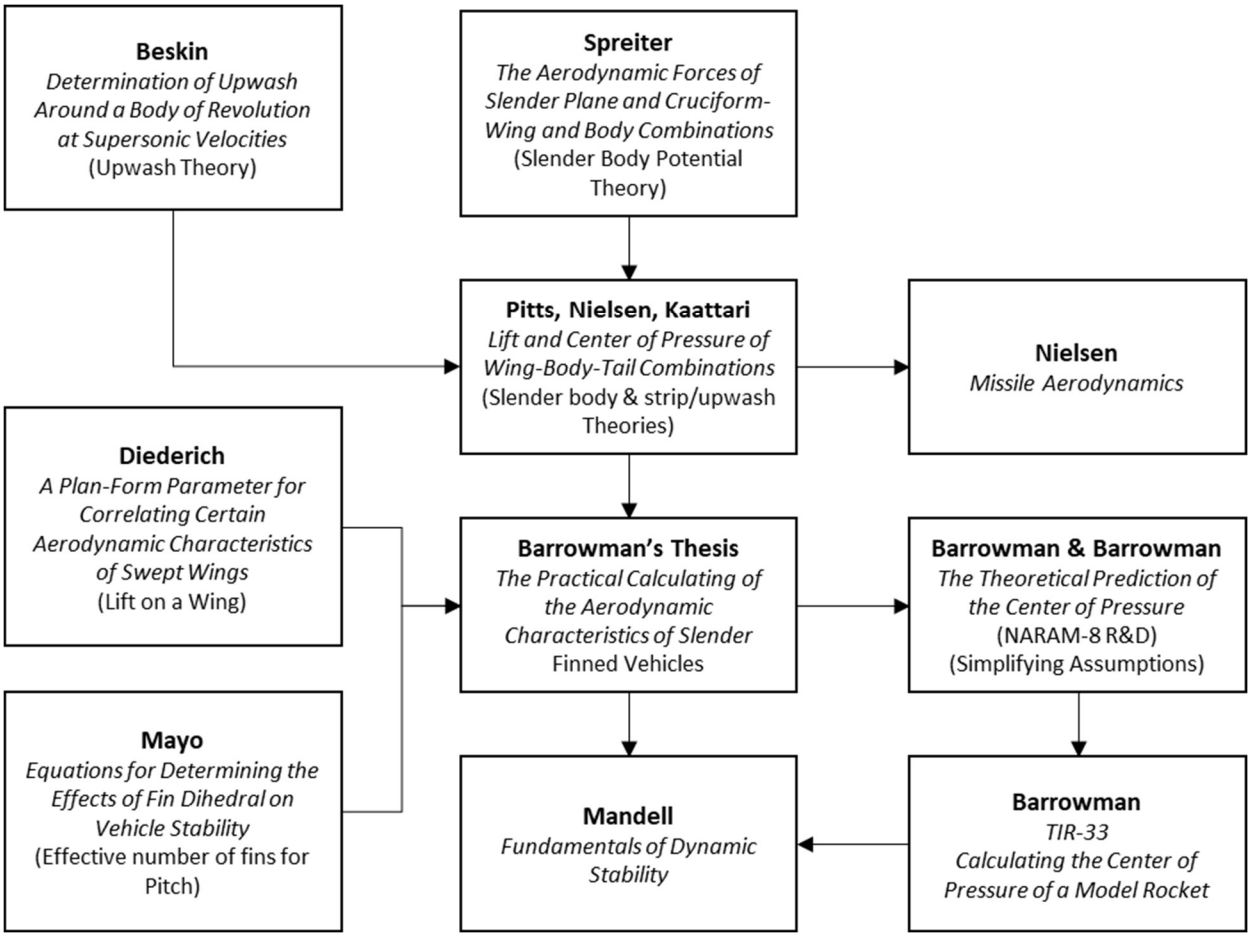

Figure 1-3 Sources for the calculation of the fin aerodynamic parameters

The equations for calculating the normal force coefficients and the center of pressure for rocket components other than the fins are best summarized in TIR-33[4], also written by James Barrowman

Also of importance are the wind tunnel tests of forward mounted canard controlled missile configurations conducted at the NASA Langley Research Center between 1978 and 1993 and reported by A.B. Blair Jr. as principal author[5]. These studies cover the measured effects of canard downwash from the forward mounted canards on the fins which has an impact on the effectiveness of the canards for roll control.

[4] (Barrowman J. , 1968).

[5] (Blair A. B., 1978), (Blair, Allen, & Hernandez, June 1983), (Blair, Dillon, & Watson, September-October 1993)

1.3 Acknowledgements

In the process of studying Jim Barrowman's thesis, I reached a point where my analysis and results for one of the aerodynamic interference factors did not agree with the results shown in his thesis. I sent my analysis and conclusions to Jim, and he very graciously reviewed it and sent me a helpful reply. I am very appreciative of Jim's taking the time to do this.

I would also like to thank Jim Jarvis for all the information he has shared about his vertical orientation flights. A year after starting my vertical orientation project at the beginning of 2022, I saw Jim's presentation at vNARCON 2023 on his vertical orientation system. I connected with Jim shortly afterward and started doing some control system modeling for his flights. The flight data I have gotten from Jim over the past 3 years has been a big help in completing and validating this modeling work.

2 Background

2.1 Lift, Drag, and Rotational Moment

When a body is inclined by an angle-of-attack, α_{at} to the direction of the oncoming airstream vector, a lift force, drag force, and rotational moment are generated as shown in Figure 2-1. The drag force is defined as the force vector that is in the direction of the oncoming airstream and pushes back on the body as it moves through the airstream. The lift force is orthogonal to the direction of the oncoming airstream and pushes the body in a direction orthogonal the airstream. The lift and drag forces, in turn, create a rotational moment that may cause the body to rotate. A moment can be referenced to any point along the length of the body. For component parts, the rotational moment is often defined about the leading edge of the object.

The lift, drag, and rotational moment completely characterize aerodynamic forces on a body, so the aerodynamics of a body are often specified by these three quantities. But for describing the rotational dynamics of a rocket, the normal force and center of pressure are used, both of which can be determined from the lift and drag forces and the rotational moment.

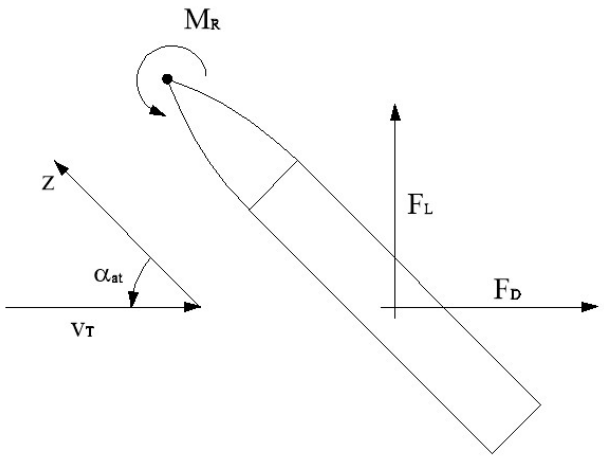

Figure 2-1 Lift, drag, and rotational moment

2.2 The Normal Force

The lift and drag forces can be resolved into a single force, F_N, that is orthogonal, or normal to the longitudinal axis of the rocket as shown in Figure 2-2.

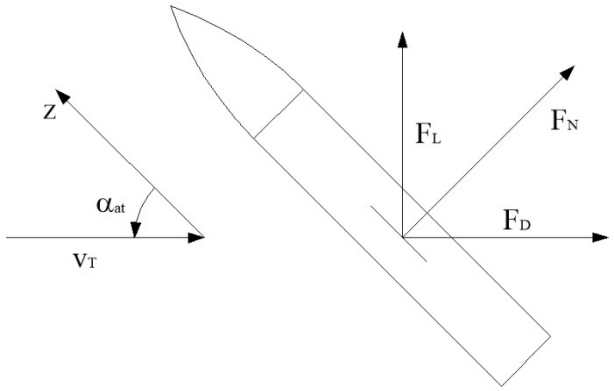

Figure 2-2 Lift, drag, and normal forces

Since any vector can be resolved into two orthogonal vectors, any two vectors can be resolved into two orthogonal vectors by adding the components from each that align. In this case, the lift and drag force vectors can be resolved into a vector aligned with the z-axis of the body, and a vector orthogonal to the z-axis, as shown in Figure 2-3. The vector orthogonal to the rocket's z-axis is the normal force that causes the rocket to rotate. The component aligned with the z-axis has no impact on the rocket's rotation and is not needed for the rotational model.

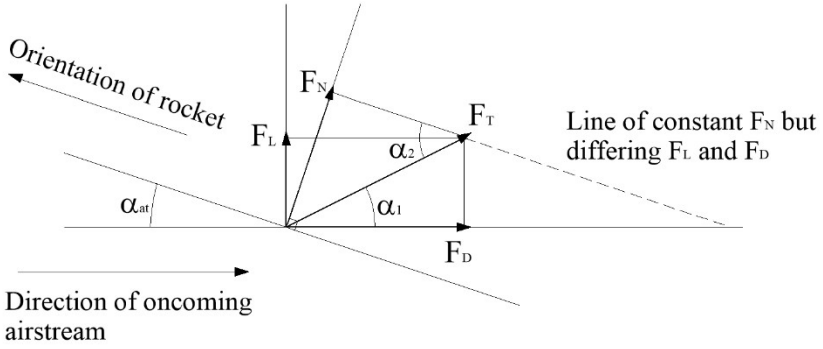

Figure 2-3 Lift, drag, and normal forces

Deriving the normal force from Figure 2-3

$$\alpha_1 = \text{atan}\left(\frac{F_L}{F_D}\right)$$

$$\alpha_2 = 90^\circ - \left(90^\circ - \left(\alpha_{at} + \alpha_1\right)\right)$$

$$\alpha_2 = \alpha_{at} + \alpha_1$$

$$F_T = \sqrt{F_L{}^2 + F_D{}^2}$$

$$F_N = F_T \cdot \sin\left(\alpha_2\right)$$

$$F_N = \sqrt{F_L{}^2 + F_D{}^2} \cdot \sin\left(\operatorname{atan}\left(\frac{F_L}{F_D}\right) + \alpha_{at}\right) \tag{2.2-1}$$

The lift and drag forces cannot be determined uniquely from the normal force alone, as described in equation (2.2-1) . Instead, the normal force describes a range of lift and drag forces that can be resolved into that normal force. The force orthogonal to the normal force is also needed to determine the lift and drag forces uniquely from the normal force.

For small angles-of-attack, Figure 2-3 shows the normal force nearly aligns with the lift force, so

$$F_N \simeq F_L \tag{2.2-2}$$

Equation (2.2-1) gives the same result with $\alpha_{at} = 0$, as expected.

2.3 The Center of Pressure

The center of pressure of a body is the point where the sum of the aerodynamic forces on either side of that point are balanced, and the rotational moment is zero. If there are multiple forces applied along the length of a body, then the total normal force is just the sum of all those individual forces, but the location of the center of pressure will depend upon where each of those individual forces is applied.

To find the rotational moment about any point along the z-axis of the rocket due to the normal force, the normal force is multiplied by the distance between that point and the center of pressure, the location on the rocket where the rotational moment is zero. That distance is the moment arm.

The center of pressure can be determined from the total normal force and the rotational moment about a given location along the body. If the rotational moment is referenced to the front of the body, the center of pressure, L_{CP}, can be determined from the moment equation as

$$M_R = F_N \cdot L_{CP} \Rightarrow L_{CP} = \frac{M_R}{F_N} \simeq \frac{M_R}{F_L} \tag{2.3-1}$$

where the normal force can be approximated by the lift force for small angles-of-attack as shown above.

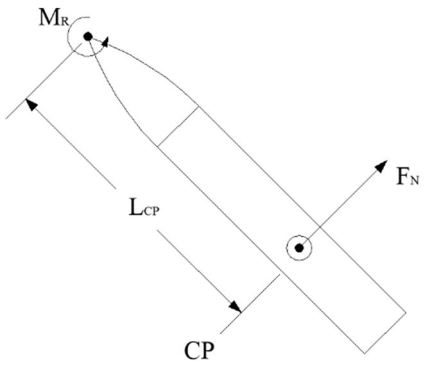

Figure 2-4 Center of pressure from zero reference rotational moment and normal force

The center of pressure of the overall rocket is determined from the normal force coefficients (see Section 2.4) and centers of pressure of the components making up the rocket by dividing the force coefficient weighted sum of the individual center of pressure locations by the sum of the force coefficients. This is the weighted average location of all the applied forces.

$$L_{CP} = \frac{C_{N1} \cdot L_{CP1} + C_{N2} \cdot L_{CP2} + \cdots}{C_{N1} + C_{N2} + \cdots} \tag{2.3-2}$$

The center of pressure locations are normally referenced from the tip of the nosecone. For example, for the fins, the location of the center of pressure is the distance from the tip of the nosecone to the location of the forward root edge of the fin plus the distance from the forward root edge to the fin's center of pressure.

In flight, the rocket rotates about its center of gravity, so the center of gravity is the reference point used for the rotational moment of the rocket. As shown in Figure 2-5, the relationship between the normal force and the rotational moment about the center of gravity is given by

$$M = F_N \cdot \left(L_{CP} - L_{CG} \right) \tag{2.3-3}$$

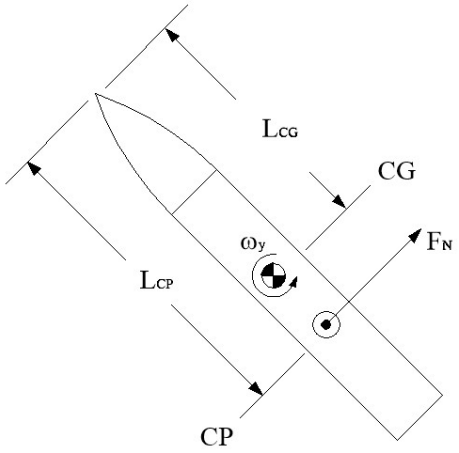

Figure 2-5 Normal force and center of pressure

2.4 Aerodynamic Forces and Force Coefficients

The aerodynamic force on a body can be expressed in the form[6]

$$F = \frac{\rho}{2} \cdot A_r \cdot {v_T}^2 \cdot C_F \tag{2.4-1}$$

which says that the force on an object due to an oncoming airstream of velocity, v_T , is proportional to the density of the air times the square of the air velocity. The constant of proportionality, C_F , is a dimensionless quantity known as the force coefficient. The force coefficient is dependent only on the shape of the body, and not its absolute size. To make the force coefficient independent of the object's size, it is normalized by the cross sectional area of the rocket, which also makes the force coefficient dimensionless. The force coefficient must then be multiplied by the rocket's cross sectional area to calculate the actual force. For the forces of interest, the drag force, the lift force, and the normal force, the following equations apply

$$F_D = \frac{\rho}{2} \cdot A_r \cdot {v_T}^2 \cdot C_D \tag{2.4-2}$$

$$F_L = \frac{\rho}{2} \cdot A_r \cdot {v_T}^2 \cdot C_L \tag{2.4-3}$$

[6] (McCormick, 1995, p. p 28)

$$F_N = \frac{\rho}{2} \cdot A_r \cdot {v_T}^2 \cdot C_N \tag{2.4-4}$$

The force coefficients are nonlinear functions of the angle-of-attack of the oncoming airstream. But, at small angles-of-attack, the force coefficients can be linearized. The drag coefficient is roughly a cosine function of the angle-of-attack, and the lift force is roughly a sine function of the angle-of-attack[7]. For small angles-of-attack, the drag coefficient is presumed to be a constant ($\cos(\alpha)\big|_{\alpha \simeq 0} = 1$), and the lift force, and therefore the normal force, is approximately proportion to the angle-of-attack, where $\sin(\alpha)\big|_{\alpha \to 0} \simeq \alpha$. Then

$$C_D \simeq 1 \tag{2.4-5}$$

$$C_L \simeq C_{L\alpha} \cdot \alpha_{at} \tag{2.4-6}$$

$$C_N \simeq C_{N\alpha} \cdot \alpha_{at} \tag{2.4-7}$$

and

$$F_D \simeq \frac{\rho}{2} A_r \cdot {v_T}^2 \cdot C_D \tag{2.4-8}$$

$$F_L \simeq \frac{\rho}{2} A_r \cdot {v_T}^2 \cdot C_{L\alpha} \cdot \alpha_{at} \tag{2.4-9}$$

$$F_N \simeq \frac{\rho}{2} A_r \cdot {v_T}^2 \cdot C_{N\alpha} \cdot \alpha_{at} \tag{2.4-10}$$

where $C_{L\alpha}$ and $C_{N\alpha}$ are the lift and normal force coefficient derivatives and are entirely dependent on the geometry of the body.

2.5 Axis Conventions in 3-Dimensions

Yaw, pitch, and roll are used to label the three distinctly different axes of an airplane. Yaw, pitch, and roll are also used to describe three rotational axes of a rocket. For a rocket, roll is used to label the longitudinal axis of the rocket as shown in Figure 2-6. Due to the symmetry of a simple rocket, there is usually no difference between the geometry of the yaw and pitch axes. By NASA's convention[8], a right hand rotation from the yaw axis to the pitch axis gives the direction of the roll axis. For the coordinate system of the rocket, the lower case axes labels x, y, and

[7] (Allen & Perkins, 1951)

[8] (Rocket Rotations, 2023)

z are used in this paper. If z is used for the longitudinal axis with the axis pointing toward the front of the rocket, then yaw maps to x, pitch maps to y, and z maps to roll.

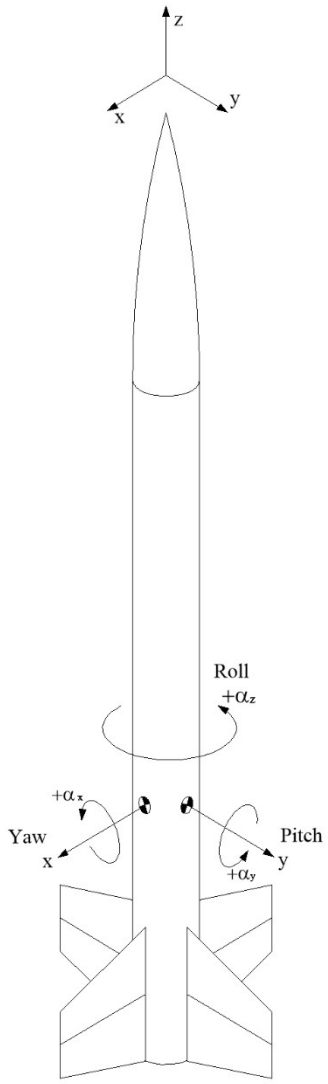

Figure 2-6 Yaw, pitch, and roll axes of a rocket

Since a rocket is symmetrical about its pitch and yaw axes, the magnitude of the pitch and yaw aerodynamic parameters will be the same, but the signs of the pitch and yaw forces will differ due to the symmetry of the axis system. Assigning the correct signs to all the forces, moments, and rotations is very important when constructing a 3-D flight model.

Figure 2-7 shows the axis conventions used in this paper for forces, moments, and rotations in three dimensions. A vector aligned with the x-axis is denoted as an x-axis vector, and a rotation about the y-axis is denoted as a y-axis angle or rotation.

For the pitch rotation shown in the left hand diagram of Figure 2-7, an oncoming airstream vector that has both z and x-axis components produces a normal force aligned with the x-axis. The angle-of-attack is the angle between the z-axis of the rocket and the direction of the oncoming airstream vector. This paper defines the rotational direction of the angle-of-attack as being the direction of the angle rotation from the z-axis of the rocket to the oncoming airstream vector, so, in this case, the angle-of-attack is a positive angle about the y-axis that results in a normal force aligned with the negative x-axis. If the rotation point is located at the y-axis, and the negative normal force is applied above the y-axis rotation point, then the positive angle-of-attack that produced the negative x-axis normal force produces a negative rotational moment about the y-axis which causes a negative rotation about the y-axis.

For the yaw rotation shown in the right hand diagram of Figure 2-7, an oncoming airstream vector that has both z and y-axis components produces a normal force aligned with the y-axis. The angle-of-attack is a positive angle about the x-axis that results in a normal force alighted with the positive y-axis. If the rotation point is located at the x-axis, and the positive normal force is applied above the x-axis rotation point, then the positive angle-of-attack that produced the positive y-axis normal force produces a negative rotational moment about the x-axis which causes a negative rotation about the x-axis.

For both pitch and yaw, the sign of the moments and the rotation directions is opposite the sign of the angle-of-attack. If the normal forces are applied below the point of rotation, then the sign of the moments and rotation directions is the same as the sign of the angle-of-attack. The sign of the normal force depends on whether it is a pitch or yaw rotation, due to the symmetry of the axes. Although the magnitude of the pitch and yaw normal forces are the same, the signs of those forces will be different.

.

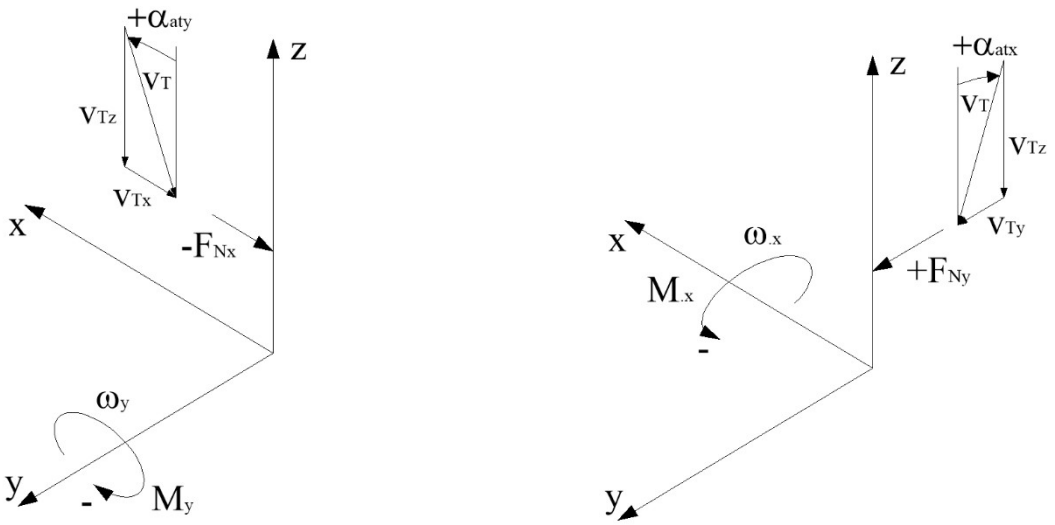

Figure 2-7 Convention for angle-of-attack angles, normal forced, moments, and axis rotations

2.6 Fin Geometry Nomenclature and Parameters

Figure 2-8 shows the fin geometry used for the aerodynamic parameter calculations in this paper. The key parameters used to describe the fin geometry, consistent with the nomenclature used by Barrowman[9] and Mandell[10], are the root edge length, c_r, tip edge length, c_t, span, s, and sweep length, c_b. Some applications such as RockSim use the sweep angle, Γ_{sweep}, rather than the sweep length. Others use the coordinate points $(0,0)$ (x_1, s) (x_2, s) $(x_3, 0)$ to describe the endpoints of the three line segments. This paper will use the first set of parameters to be consistent with Barrowman and Mandell.

The longitudinal fin dimensions are measured from the forward root edge of the fin reward, as indicated by the z-axis in Figure 2-8. This is consistent with all other rocket geometry parameters such as the location of the center of pressure and gravity, which are positive values measured rearward from the tip of the nosecone. Radially, the z-axis is the centerline of the rocket. This rocket geometry z-axis aligns with the rocket frame of reference z-axis described in Section 2.5, but is oriented in the opposite direction. This is to be consistent with the convention established by the other references mentioned above. Because this z-axis is used only to determine the geometry of

---

[9] (Barrowman J. S., The Practical Calculation of the Aerodynamic Characteristics of Slender Finned Vehicles, Master's Thesis, 1967, pp. 7 Figure 3-2)

[10] (Mandell, Caporaso, & Bengen, 1973, p. 194 Figure 36)

the rocket, it is separate from the rocket frame of reference z-axis, and the use of the two does not conflict. Note that the radial distance, r, is measured from the centerline of the rocket, not the root edge of the fin.

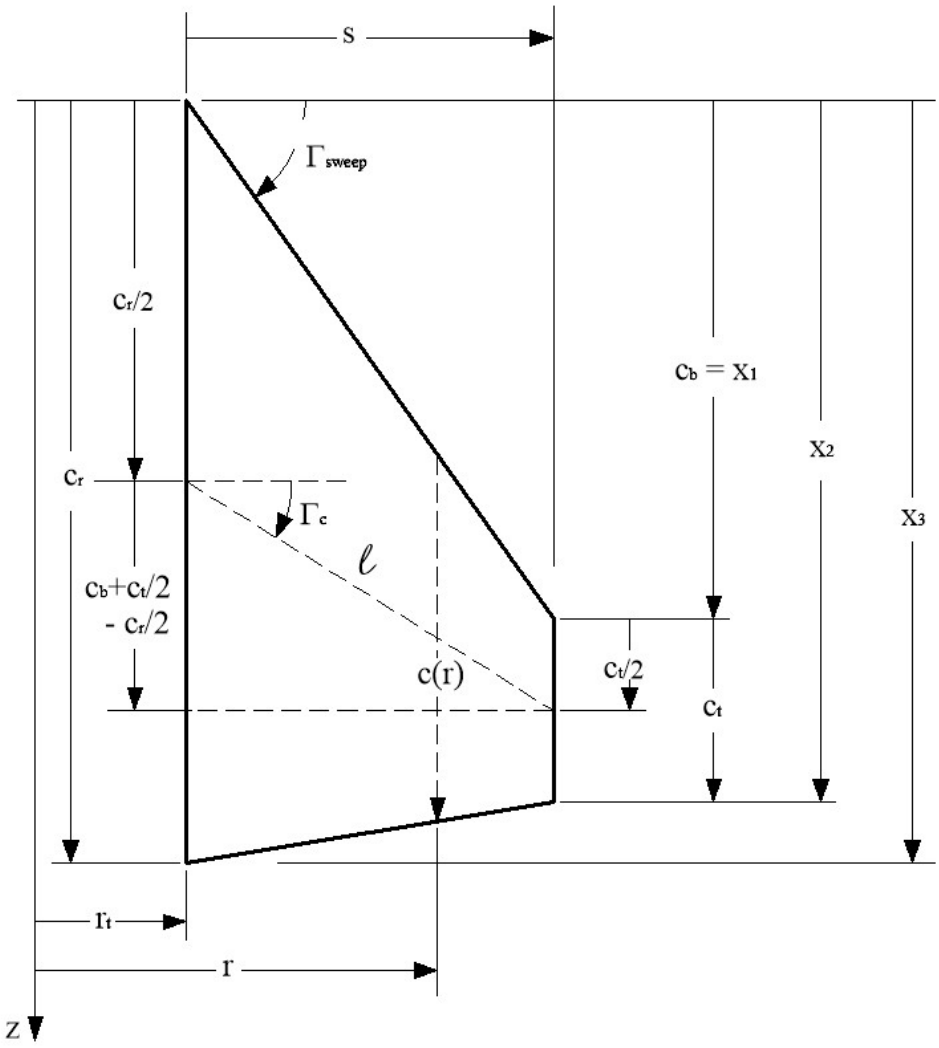

Figure 2-8 Nomenclature for describing the geometry of a fin

Figure 2-9 shows that both non-swept and swept fins are possible using these descriptive parameters.

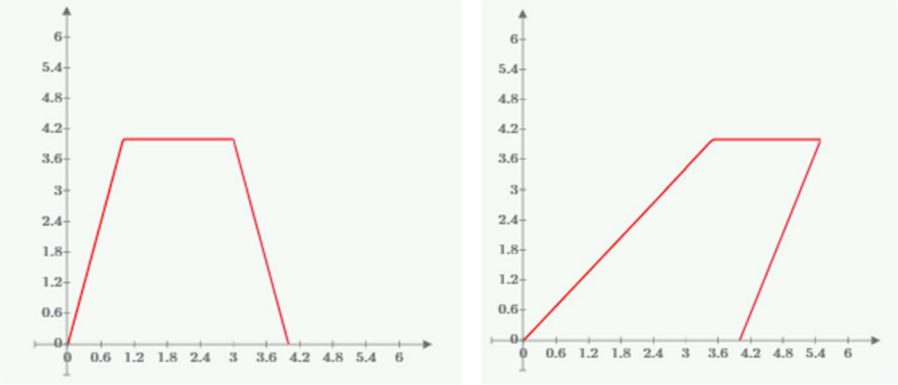

$c_r = 4in$
$c_t = 2in$
$c_b = 1in$
$s = 4in$

$c_r = 4in$
$c_t = 2in$
$c_b = 3.5in$
$s = 4in$

Figure 2-9 Examples of fin geometries and the related parameters

The sweep angle of the leading edge of the fin is

$$\Gamma_{sweep} = \text{atan}\left(\frac{c_b}{s}\right) \tag{2.6-1}$$

The length of the midpoint centerline is

$$\ell = \sqrt{s^2 + \left(c_b + \frac{c_t}{2} + \frac{c_r}{2}\right)^2} \tag{2.6-2}$$

The angle of the midpoint centerline is

$$\Gamma_c = a\cos\left(\frac{s}{\ell}\right) \tag{2.6-3}$$

The line that defines the leading edge of the fin, measured positively along the z-axis of Figure 2-8, from the tip of the root edge, is

$$z_{le} = \frac{c_b}{s} \cdot r \tag{2.6-4}$$

and the line defining the trailing edge is

$$z_{te}(r) = c_r - \frac{c_r - (c_b + c_t)}{s} \cdot r \tag{2.6-5}$$

These lines are used as the limits of integration when integrating over the area of the fin.

The length of the chord line at any radius can be determined geometrically or by doing the integral along the z-axis from the leading edge of the fin to the trailing edge of the fin. The radius r must be offset by the radius of the body tube, r_t, in the limits of integration since r is measured from the z-axis centerline of the rocket.

$$c(r) = \int_{\frac{c_b}{s}\cdot(r-r_t)}^{c_r - \frac{c_r-(c_b+c_t)}{s}\cdot(r-r_t)} 1 \cdot dz = c_r - \frac{(r-r_t)\cdot(c_r - c_t)}{s} \tag{2.6-6}$$

The area of a fin is

$$A_f = \int_{r_t}^{r_t+s} \int_{\frac{c_b}{s}\cdot(r-r_t)}^{c_r - \frac{c_r-(c_b+c_t)}{s}\cdot(r-r_t)} 1 \cdot dz \cdot dr = \int_{r_t}^{r_t+s} c(r) \cdot dr = s \cdot \frac{c_t + c_r}{2} \tag{2.6-7}$$

The aspect ratio of the fins is used in the equation for the normal force coefficient. The aspect ratio for a rectangular wing is the span divided by the chord length. Diederich[11] defines the aspect ratio for a tapered wing as the tip-to tip span of a wing divided by the average chord. Defining this in terms of the span of a single fin, or half a wing, the aspect ratio is twice the span to average chord ratio of a single fin.

$$AR = \frac{2 \cdot s}{c_{avg}} \tag{2.6-8}$$

The average chord for a tapered fin can be calculated by

$$c_{avg} = \frac{A_f}{s} \tag{2.6-9}$$

So, for a tapered fin, combining equations (2.6-8) and (2.6-9), the aspect ratio is

[11] (Diederich, 1951, p. 2)

$$AR = \frac{2 \cdot s^2}{A_f} = \frac{4 \cdot s}{c_r + c_t} \tag{2.6-10}$$

Mandell[12] states the aspect ratio as $\frac{2 \cdot s}{c_r + c_t}$, which would make it equivalent to the aspect ratio for a single fin. Barrowman[13] uses Diederich's definition. Since the equations in Mandell that use the aspect ratio are the same as the equivalent equations in Barrowman, Mandell's definition of aspect ratio must be off by a factor of 2.

There are two ratios that are used in some of the aerodynamic parameter equations to simplify the equations. τ is the ratio of the span of the fin from the centerline of the rocket (fin span plus body tube radius) to the radius of the body tube.

$$\tau = \frac{s + r_t}{r_t} \tag{2.6-11}$$

λ is the ratio of the fin tip length to the root length. It indicates the pointiness of the fin geometry

$$\lambda = \frac{c_t}{c_r} \tag{2.6-12}$$

Both τ and λ are dimensionless. The advantage of expressing certain aerodynamic parameters, in particular the interference factors, in terms of τ and λ, is it shows that those expressions are dependent on the shape but not the absolute dimensions of the fins.

2.7 Strip Theory

The lift and normal force on a fin are functions of the angle-of-attack. Strip theory can be used to determine the total lift or normal force on a fin when the angle-of-attack changes radially as a function of the distance from the z-axis centerline of the rocket. This is the case for the radial forcing moment and the tail body interference factor (both covered in Section 3). For these forces, it is just the angle-of-attack that changes as a function of the radial distance from the center line of the rocket, due to the tangential velocity of the airstream, which changes with the

[12] (Mandell, Caporaso, & Bengen, 1973, p. 194)

[13] (Barrowman J. S., 1967, p. 3)

radius for a rolling rocket. For the radial damping moment, there is a radial moment arm that is a function of the radius, in addition to the change in angle-of-attack, and strip theory works for this as well.

Strip theory divides the fin into a series of thin strips as shown in Figure 2-10. The force on each strip is calculated using the value of the angle-of-attack or other radially dependent force function at the center of each strip. Then the forces on each of the strips are added to determine the total force on the fin. The narrower each of the strips, the more accurate the result. In the limit where the width of each strip goes to zero, the summation becomes an integral over the span of the fin.

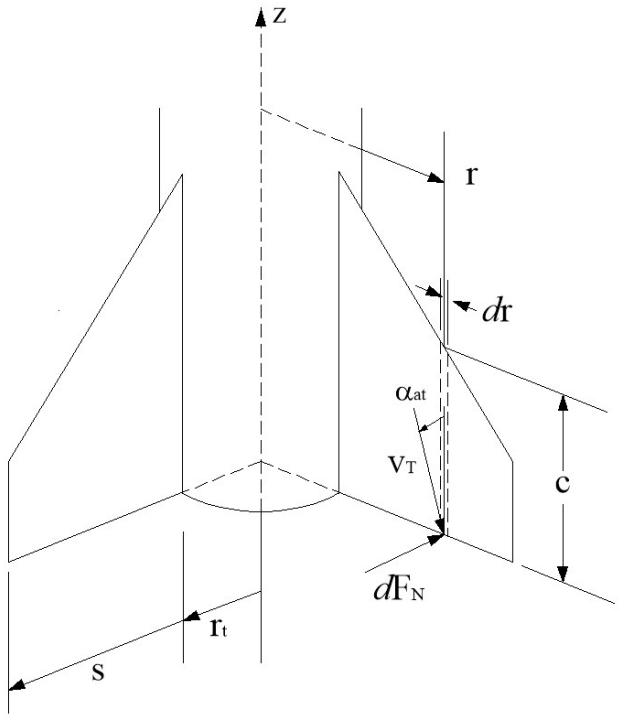

Figure 2-10 Angle-of-attack and incremental force on a narrow strip at radius *r*

Representing the angle-of-attack as a function of the radius, $\alpha_{at}(r)$, and allowing the width of each strip goes to zero, the incremental force on each strip is the total normal force for the angle-of-attack at that radius times the portion of the total fin area for that strip divided by the total fin area, A_f. The incremental area of a strip is the strip's length times its width, $c(r) \cdot dr$.

$$dF_N = -\frac{\rho}{2} \cdot v_{Tz}{}^2 \cdot A_r \cdot \alpha_{at}(r) \cdot C_{N\alpha R} \cdot \frac{c(r) \cdot dr}{A_f} \tag{2.7-1}$$

The total force on the fin is then determined by the integral of the incremental force over the area of the fin, using the angle-of-attack for each strip, where the limits of integration on the radial axis are the radius of the body tube, r_t to the radius of the tip of the fin, $r_t + s$. Replacing the fin area with its integral expression in terms of the chord line length, $c(r)$, from equation (2.6-7), the total normal force is

$$F_N = -\frac{\rho}{2} \cdot {v_{Tz}}^2 \cdot A_r \cdot C_{N\alpha R} \cdot \frac{\int_{r_t}^{r_t+s} \alpha_{at}(r) \cdot c(r) \cdot dr}{\int_{r_t}^{r_t+s} c(r) \cdot dr} \tag{2.7-2}$$

Mathcad, the tool used for all the modeling done for this paper, can be used to perform the integral calculations of equation (2.7-2) symbolically in order to obtain a closed form solution for the aerodynamic parameter. Mathcad makes it much easier to evaluate the integrals than the geometric process Barrowman used without having this tool.

3 Control Fin Aerodynamic Parameters

3.1 Normal Force Coefficient Derivative for a Single and Multiple Fins

The steps for calculating the normal force coefficient derivative for the fins are given by Barrowman[14] based on the work of Diederich[15]. The normal force coefficient derivative for a single fin is[16]

$$C_{N\alpha 1f} = \frac{2 \cdot \pi \cdot AR \cdot \left(\frac{A_f}{A_r} \right)}{2 + \sqrt{4 + \left(\frac{\beta \cdot AR}{\cos(\Gamma_c)} \right)^2}} \tag{3.1-1}$$

where β is determined from the Mach number, M , by

$$\begin{aligned} \beta\big|_{M<1} &= \sqrt{1 - M^2} \\ \beta\big|_{M>1} &= \sqrt{M^2 - 1} \end{aligned} \tag{3.1-2}$$

For velocities well below Mach 1, equation (3.1-1) can be simplified to

$$C_{N\alpha 1f} = \frac{2 \cdot \pi \cdot AR \cdot \left(\frac{A_f}{A_r} \right)}{2 + \sqrt{4 + \left(\frac{AR}{\cos(\Gamma_c)} \right)^2}} \tag{3.1-3}$$

The next step is to calculate the effectiveness of multiple fins that are spaced around the body of the rocket. When a rocket is at a pitch angle-of-attack relative to the oncoming airstream, the velocity of the airstream, v_T , can be broken down into two orthogonal components, v_{Tx} and v_{Tz} as shown in Figure 3-1, where v_{Tx} is the component of the airstream orthogonal to the longitudinal axis of the rocket.

---

[14] (Barrowman J. S., 1967, p. 3)

[15] (Diederich, 1951)

[16] (Barrowman J. S., 1967, pp. 3 eq 3-6)

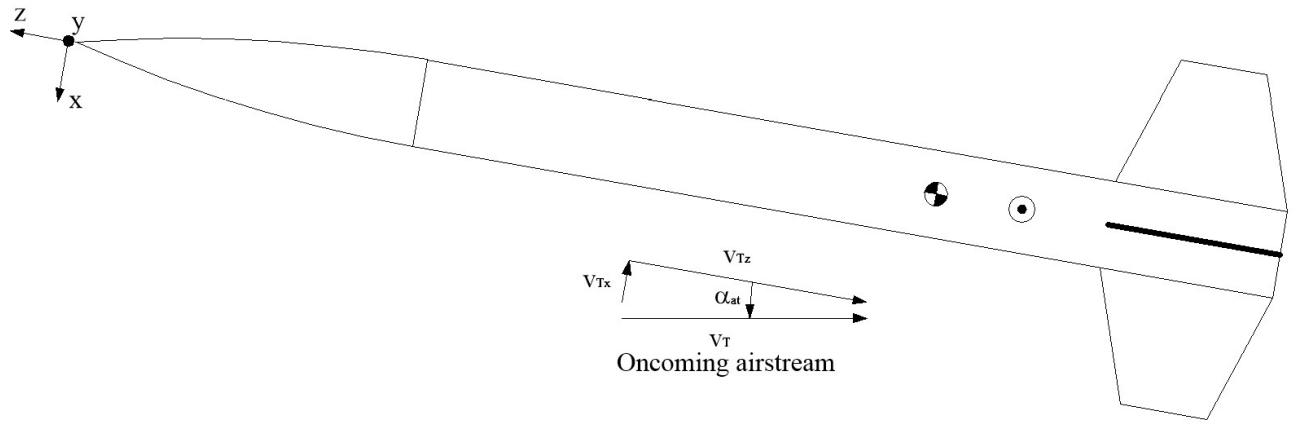

Figure 3-1 x and z-axis components of the oncoming airstream velocity

To calculate the normal force for a number of fins spaced evenly around the perimeter of the body tube, the normal force for a single fin that is at rotated away from an orthogonal orientation to the airstream by the z-axis offset angle Λ, as shown in Figure 3-2, must first be calculated.

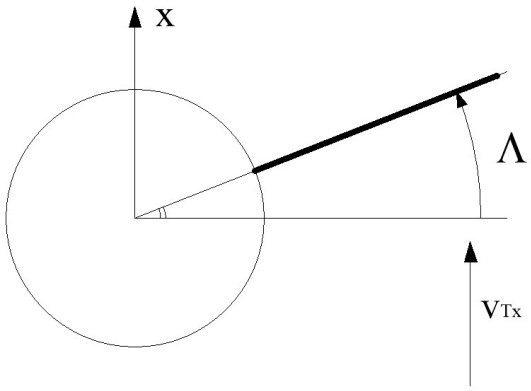

Figure 3-2 Dihedral angle of a fin

Barrowman calls the z-axis offset angle the dihedral angle[17], and gives the equation for calculating the effectiveness as

[17] (Barrowman J. S., 1967, pp. 4-5)

$$C_{N\alpha efffective} = C_{N\alpha 1 f} \cdot \cos(\Lambda)^2 \tag{3.1-4}$$

Barrowman does not show the derivation of this equation but rather cites Mayo[18] as the source. Mayo's NASA memo is not available on the NTRS server, and it could not be found from a search of the internet, so the derivation of equation (3.1-4) is presented here.

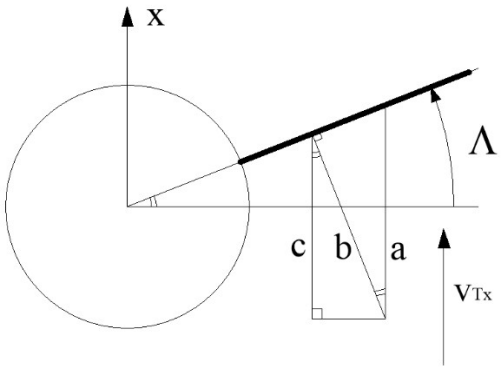

Figure 3-3 Effectiveness of a fin at a dihedral angle Λ

Figure 3-3 shows the rocket from above with the fin rotated at a dihedral angle of Λ from a position that is orthogonal to the x-axis component of the oncoming airstream. In this figure, the total oncoming airstream vector, v_T, is down into the paper. All the angles with the double arcs equal Λ° in this figure. The component of v_{Tx}, and hence v_T, that is orthogonal to the rotated fin that will create the normal force on the fin is

$$b = a \cdot \cos(\Lambda) \tag{3.1-5}$$

Since the normal force is proportional v_T, the normal force on the fin at a dihedral angle will scale as equation (3.1-5). But the normal force needed is the component of (3.1-5) that is aligned with v_{Tx} which is

$$c = b \cdot \cos(\Lambda) = a \cdot \cos(\Lambda)^2 \tag{3.1-6}$$

[18] (Mayo, 1967)

so the normal force on the rocket aligned with v_{Tx} for a fin at a dihedral angle of Λ is proportional to the square of the cosine of the dihedral angle, as given by equation (3.1-4)

The total normal force on the fin tail section is the sum of the effective normal forces on each of the fins as scaled by equation (3.1-4). For 3 fins, the total force coefficient derivative is

$$C_{N\alpha T3f} = C_{N\alpha 1f} \cdot \cos(\Lambda)^2 + C_{N\alpha 1f} \cdot \cos\left(\Lambda + \frac{1}{3} \cdot 2 \cdot \pi\right)^2 + C_{N\alpha 1f} \cdot \cos\left(\Lambda + \frac{2}{3} \cdot 2 \cdot \pi\right)^2 = \frac{3}{2} \cdot C_{N\alpha 1f} \qquad (3.1\text{-}7)$$

and for 4 fins, the total force coefficient derivative is

$$\begin{aligned} C_{N\alpha T4f} &= C_{N\alpha 1f} \cdot \cos(\Lambda)^2 + C_{N\alpha 1f} \cdot \cos\left(\Lambda + \frac{1}{4} \cdot 2 \cdot \pi\right)^2 \\ &+ C_{N\alpha 1f} \cdot \cos\left(\Lambda + \frac{1}{2} \cdot 2 \cdot \pi\right)^2 + C_{N\alpha 1f} \cdot \cos\left(\Lambda + \frac{3}{4} \cdot 2 \cdot \pi\right)^2 = 2 \cdot C_{N\alpha 1f} \end{aligned} \qquad (3.1\text{-}8)$$

These equations space the fins equally around the perimeter of the rocket, where Λ can be any starting offset angle. For any number of fins greater than two, the general equation is

$$C_{N\alpha Tf} = \sum_{n=0}^{N-1} C_{N\alpha 1f} \cdot \cos\left(\Lambda + \frac{n}{N} \cdot 2 \cdot \pi\right)^2 = \frac{N}{2} \cdot C_{N\alpha 1f} \qquad (3.1\text{-}9)$$

where N is the total number of fins. The initial angle offset, Λ, drops out of the summation when the number of fins is greater than 2. Barrowman evaluates 3 and 4 fins[19], but equation (3.1-9) says that the normal force on the tail section is independent of the z-axis offset rotation angle of the rocket for any number of evenly spaced fins greater than 2.

If the pitch normal force coefficient were not independent of the starting rotation, then the pitch normal force would be a function of the rockets z-axis rotation, and that cross coupling would cause the rocket to oscillate in pitch and yaw as it rolls. Figure 3-4 shows the individual normal force coefficient derivatives as a function of Λ for 3 fins, and Figure 3-5 shows the individual normal force coefficient derivatives for 4 fins, as a function of the offset angle. Both graphs also show the constant value of the sum of the individual fin coefficients. For 4 fins, opposite fins map on top of each other, so the equivalent of 2 out of 4 fins are effective at any rotational orientation. For 3 fins total, 1.5 fins are effective at any rotational orientation.

[19] (Barrowman J. S., 1967, p. 4)

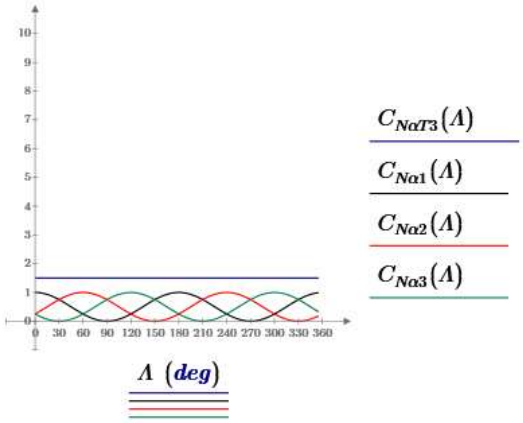

Figure 3-4 The normalized normal force on each fin as a function of the z-axis offset angle for 3 fins

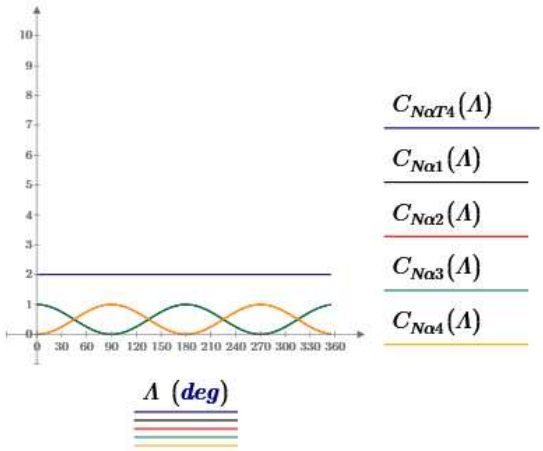

Figure 3-5 The normalized normal force on each fin as a function of the z-axis offset angle for 4 fins

Substituting equation (3.1-9) into equation (3.1-3) gives the normal force coefficient derivative for the complete tail section with N fins as

$$C_{N\alpha Tf} = \frac{N \cdot \pi \cdot AR \cdot \left(\frac{A_f}{A_r} \right)}{2 + \sqrt{4 + \left(\frac{AR}{\cos(\Gamma_c)} \right)^2}} \tag{3.1-10}$$

This is the same as the tail normal force coefficient derivative from Barrowman[20]. In Barrowman's NARAM-8 report[21] in and TIR-33[22], the total normal force coefficient derivative is given as

$$C_{N\alpha Tf} = \frac{N \cdot \pi \cdot \left(\frac{s}{D_r}\right)^2}{1 + \sqrt{1 + \left(\frac{2 \cdot \ell}{c_r + c_t}\right)^2}} \tag{3.1-11}$$

which is the same as equation (3.1-10) expressed using different fin parameters (see Section 2.6).

The normal force coefficient derivative for roll for a single fin is the same as the normal force coefficient derivative for pitch for a single fin, as given by equation (3.1-3). But for multiple fins, where opposite fins are rotated in opposite rotational directions (see Figure 3-19), all the fins contribute to the total roll normal force, so the normal force coefficient derivative for *N* fins is

$$C_{N\alpha Rf} = N \cdot C_{N\alpha 1 f} \tag{3.1-12}$$

which is twice the total pitch normal force coefficient derivative for the same number of fins. Combining equation (3.1-12) with equation (3.1-3) gives the roll normal force coefficient as

$$C_{N\alpha Rf} = \frac{2 \cdot N \cdot \pi \cdot AR \cdot \left(\frac{A_f}{A_r}\right)}{2 + \sqrt{4 + \left(\frac{AR}{\cos(\Gamma_c)}\right)^2}} \tag{3.1-13}$$

3.2 Tail-Body Interference due to Body Angle-of-Attack

There is an increase in the angle-of-attack of the airstream as it passes over the fins due to the presence of the body tube. That increase in angle-of-attack increases the normal force on the fins. This is called tail-body interference.

---

[20] (Barrowman J. S., 1967, pp. 6 eq 3-11)

[21] (Barrowman & Barrowman, 1966, p. 26 eq 59)

[22] (Barrowman J. , 1968, p. 11)

When the rocket is at an angle-of-attack to the oncoming airstream, the airstream velocity vector can be resolved into a component aligned with the z-axis of the rocket and a component orthogonal to the z-axis aligned with the x-axis as shown in Figure 3-6.

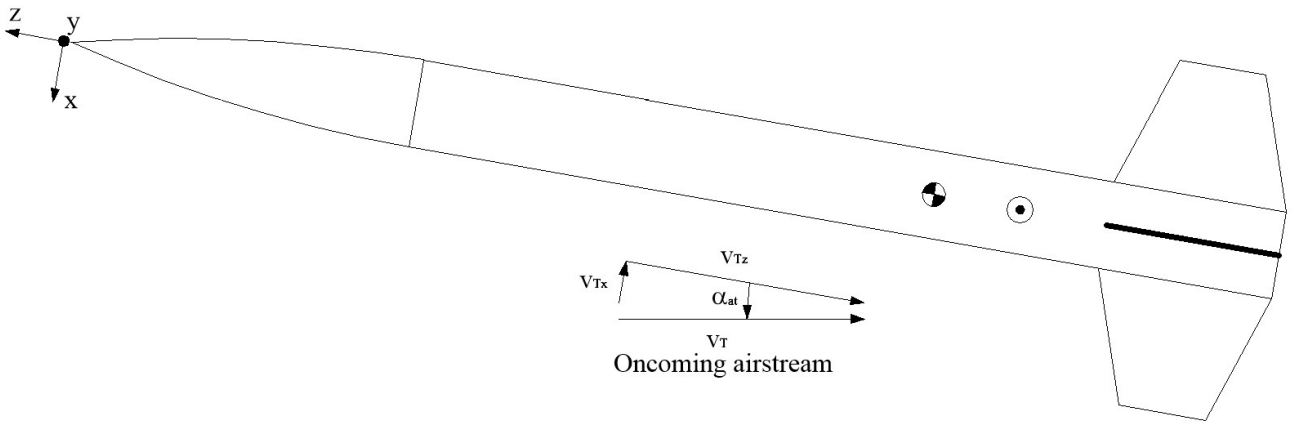

Figure 3-6 x and z-axis components of the oncoming airstream for a rocket at an angle-of-attack

As shown by Spreiter[23], the component of the oncoming airstream forced to go around the body tube is shown in Figure 3-7. Since the path around the body tube is longer than a straight path, the velocity of the air must increase as it passes by the body tube.

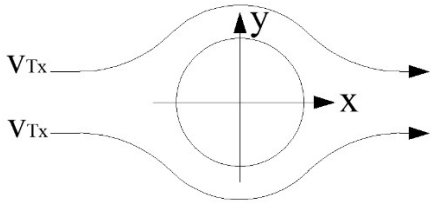

Figure 3-7 x-axis component of the oncoming airstream going around the body tube

Beskin[24] gives the x-axis velocity as a function of the distance from the body tube as

[23] (Spreiter, 1950, p. 273)

[24] (Beskin, 1946, p. 3)

$$v_{Tx}{}' = v_{Tx} \cdot \left(1 + \frac{r_t^2}{r^2}\right) \tag{3.2-1}$$

The modified airstream velocity near the body tube from equation (3.2-1) is shown in Figure 3-8. This says that the velocity of the air at the boundary of the body tube is twice the velocity of the ambient airstream without the body tube and that it decreases as the square of the distance from the body tube as it approaches the ambient velocity. Beskin uses the term upwash to describe this airflow over the fins.

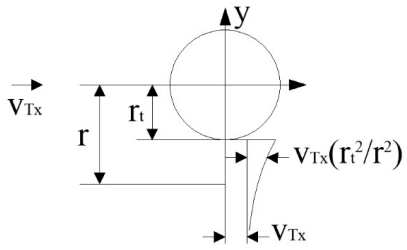

Figure 3-8 Velocity of the x-axis component as a function of the distance from the center of the body tube

The relationship between the angle-of-attack and the velocities is given by

$$\alpha_{at} = \text{atan}\left(\frac{v_x}{v_z}\right) \simeq \frac{v_x}{v_z} \tag{3.2-2}$$

Substituting equation (3.2-1) into equation (3.2-2) gives

$$\alpha_{at}\left(r\right)' = \alpha_{at} \cdot \left(1 + \frac{r_t^2}{r^2}\right) \tag{3.2-3}$$

where α_{at} is the angle-of-attack of the body tube. This is the result shown in Pits, Nielsen, & Kaattari[25].

Since the angle-of-attack with the tail body interference is a function of the radius, the total force on the fins is determined using strip theory (see Section 2.7). The fin is broken up into a number of incremental strips and the force on each individual strip is calculated using the angle-of-attack at that radius from equation (3.2-3) The total normal force for a single fin with the tail-body interference is

[25] (Pitts, Neilsen, & Kaattari, 1957, p. 570 eq 15)

$$F_{Nf}\,' = C_{N\alpha 1f} \cdot \frac{\rho}{2} A_r \cdot {v_T}^2 \cdot \alpha_{at} \cdot \frac{\int_{r_t}^{(r_t+s)} c(r) \cdot \left(1 + \frac{r_t^2}{r^2}\right) \cdot dr}{A_f} \tag{3.2-4}$$

where $c(r)$ is the fin chord length at radius r from equation (2.6-6). The tail-body interference factor is the ratio of the normal force with the tail body interference to the normal force without interference[26]. $C_{N\alpha} \cdot \frac{\rho}{2} A_r \cdot {v_T}^2 \cdot \alpha_{at}$ is common to both. Replacing the fin area, A_f, with its integral expressions (see Section 2.6) and evaluating the integrals, the tail-body interference factor is

$$K_{TBup} = \frac{\int_{r_t}^{(r_t+s)} c(r) \cdot \left(1 + \frac{r_t^2}{r^2}\right) \cdot dr}{\int_{r_t}^{(r_t+s)} c(r) \cdot dr} = \frac{\left[\begin{array}{l}(2 \cdot \lambda - 2) \cdot \tau \cdot \ln(r_t \cdot \tau) + (2 - 2 \cdot \lambda) \cdot \tau \cdot \ln(r_t) \\ + (\lambda + 1) \cdot \tau^3 - 2 \cdot \lambda \cdot \tau^2 - (\lambda + 1) \cdot \tau + 2 \cdot \lambda\end{array}\right]}{(\tau^2 - \tau) \cdot (\lambda + 1) \cdot (\tau - 1)} \tag{3.2-5}$$

where

$$\lambda = \frac{c_t}{c_r} \tag{3.2-6}$$

is the ratio of the tip chord to the root chord, and

$$\tau = \frac{s + r_t}{r_t} \tag{3.2-7}$$

is the ratio of the fin span plus the radius of the body tube to the radius of the body tube.

Barrowman[27] uses the slender-body theory tail-body interference factor equation from Pitts, Nielsen, & Kaattari[28]

---

[26] (Pitts, Neilsen, & Kaattari, 1957, p. 570 eq 16)

[27] (Barrowman J. S., 1967, pp. 31 eq 3-96) Note - eq 3-96 is missing the $+\pi/4$ in the numerator

[28] (Pitts, Neilsen, & Kaattari, 1957, p. 570 eq 14) Note – Pitts et al uses $s = s + r_t$, i.e. the body tube radius is included in s

$$K_{TBtb} = \frac{2}{\pi} \cdot \frac{\left(1+\frac{1}{\tau^4}\right) \cdot \left(\frac{1}{2} \cdot \operatorname{atan}\left(\frac{1}{2} \cdot \left(\tau - \frac{1}{\tau}\right)\right) + \frac{\pi}{4}\right) - \frac{1}{\tau^2} \cdot \left(\left(\tau - \frac{1}{\tau}\right) + 2 \cdot \operatorname{atan}\left(\frac{1}{\tau}\right)\right)}{\left(1-\frac{1}{\tau}\right)^2} \tag{3.2-8}$$

Figure 3-9 shows a plot of the upwash/strip theory Equation (3.2-5) for two values of the tip to root ratio λ, and the slender-body Equation (3.2-8), both versus the ratio of the body diameter to the span plus body diameter. The slender body theory and the upwash/strip theory results are very similar, with the upwash/strip theory curves bowing slightly upward, and the slender body theory curve bowing slightly downward. These are the same results shown in Pitts et al[29]

In their NARAM-8 R&D report, Barrowman and Barrowman[30] simplify these expressions as a line between the endpoints of equation (3.2-8). This is the function that is used in TIR-33[31]

$$K_{TBln} = 1 + \frac{1}{\tau} = 1 + \frac{r_t}{s + r_t} \tag{3.2-9}$$

Equation (3.2-9) is also plotted in Figure 3-9 which shows that it is a good approximation to the other two more complicated functions; in fact it is midway between the slender body and upwash/strip theory results.

[29] (Pitts, Neilsen, & Kaattari, 1957, p. 571 Figure 2)

[30] (Barrowman & Barrowman, 1966, p. 36 eq 77)

[31] (Barrowman J. , 1968, p. 11) K_{TB} is called K_{fb} in TIR-33

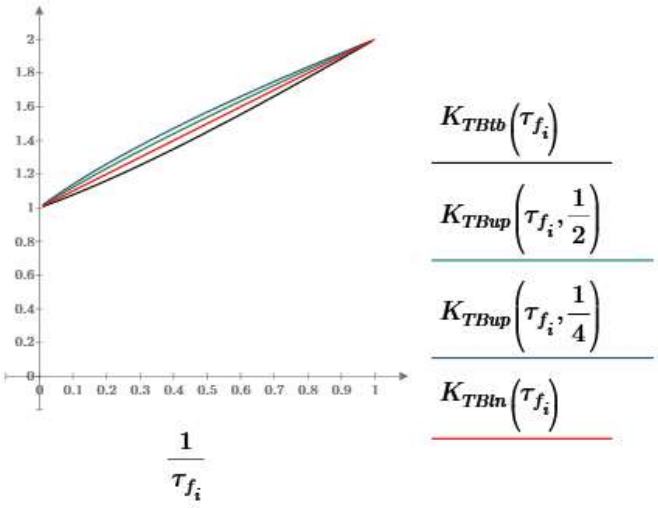

Figure 3-9 Comparison of the different tail-body interference equations vs τ

K_{TBtb} = slender body theory, K_{TBup} = strip theory for $\lambda = 1/2$ and $\lambda = 1/4$, $K_{TB\ln}$ = straight line approximation

These results show that for a λ ratio near zero, where the span is large compared to the radius of the body tube, and most of the fin is well away from the body tube, the impact of the increase in the airstream velocity and effective angle-of-attack near the body tube has little overall impact, and the tail-body multiplier factor is close to 1. For a λ ratio near 1, the span is small compared to the radius of the body tube, and most of the fin is close to the body tube, so the airstream velocity and effective angle-of-attack is close to twice the actual angle-of-attack of the body tube and fins, and the tail-body multiplier factor is close to 2.

3.3 Tail-Body Interference due to the Rotation Angle of the Fin

There is also interference from the body tube on the fins if the fins are rotated by an angle relative to the body tube. This interference is independent of the angle-of-attack of the body tube. Although Barrowman describes this interference factor as applying to canted fins that induce roll, it applies to an angled fin whether that fin's rotation is causing either a pitch or roll rotation of the rocket (Barrowman does not cover the case of pitch rotation due to canted fins).

For the interference equation[32] Barrowman references Pitts, Nielsen, and Kaattari[33] for the derivation using potential theory as strip theory does not work for this case. The tail-body interference factor due to the angle of the fin is given by

$$k_{TBf} = \frac{1}{\pi^2}\cdot\left(\begin{array}{l}\frac{\pi^2}{4}\cdot\frac{(\tau+1)^2}{\tau^2}+\frac{\pi\cdot(\tau^2+1)^2}{\tau^2\cdot(\tau-1)^2}\cdot\operatorname{asin}\left(\frac{\tau^2-1}{\tau^2+1}\right)-\frac{2\cdot\pi\cdot(\tau+1)}{\tau\cdot(\tau-1)}+ \\ \frac{(\tau^2+1)^2}{\tau^2\cdot(\tau-1)^2}\cdot\left(\operatorname{asin}\left(\frac{\tau^2-1}{\tau^2+1}\right)\right)^2-\frac{4\cdot(\tau+1)}{\tau\cdot(\tau-1)}\cdot\operatorname{asin}\left(\frac{\tau^2-1}{\tau^2+1}\right)+\frac{8}{(\tau-1)^2}\cdot\ln\left(\frac{\tau^2+1}{2\cdot\tau}\right)\end{array}\right) \tag{3.3-1}$$

Plotting equation (3.3-1), as a function $\tau = r_t/(r_t+s)$, the ratio of the fin span plus the body radius to the body radius, in Figure 3-10, it can be seen that the impact of the fin angle interference factor is small, as the factor is close to 1 for all values of τ , so this interference factor can be neglected in most cases.

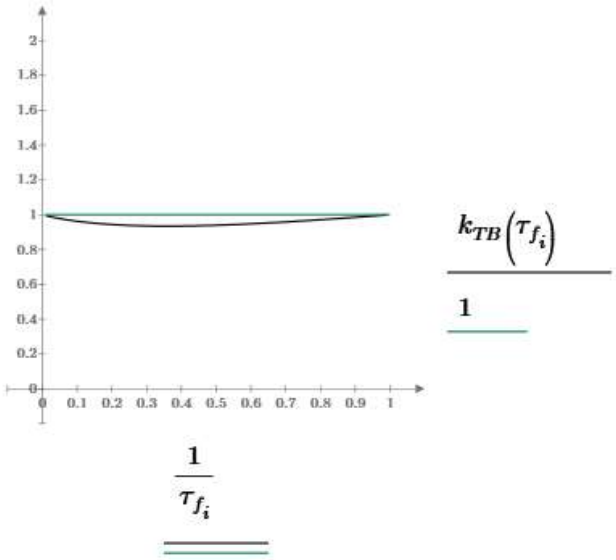

Figure 3-10 Tail-body interference factor due to the angle of the fin

[32] (Barrowman J. S., 1967, pp. 37 eq. (3-105))

[33] (Pitts, Neilsen, & Kaattari, 1957, p. 571 eq. (19) & Appendix A)

3.4 Pitch and Yaw Induced Angle-of-Attack

Once a rocket is rotating about its center of gravity, perhaps due to a wind perturbation, there is an induced angle-of-attack due to the rocket's rotation.

Figure 3-11 shows that when a rocket is rotating longitudinally about its center of gravity, in this case a pitch rotation, the location at the center of pressure of the fins rotates with a tangential velocity of $v_{\omega y}$.

Figure 3-11 Pitch rotation about the center of gravity

The tangential velocity at the center of pressure of the fins is given by

$$v_{\omega y} = \omega_y \cdot \left(L_{CPf} - L_{CG} \right) \tag{3.4-1}$$

for ω_y in units of rad/s. For a positive direction of rotation and a positive tangential velocity, the rocket sees an induced wind vector that is equal in velocity and opposite in direction from the rotational velocity, as shown in Figure 3-12.

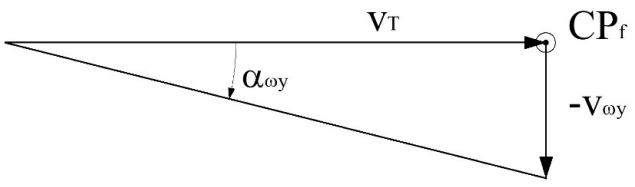

Figure 3-12 Induced air angle-of-attack due to rocket's rotation

If the velocity of the airstream that is incident on the rocket is v_T , then the induced angle-of-attack due to the rocket's rotation rate for small angles is

$$\alpha_{\omega y} \simeq \text{atan}\left(\frac{-v_{\omega y}}{v_T}\right) \simeq \frac{-v_{\omega y}}{v_T} = \frac{-\omega_y \cdot \left(L_{CPf} - L_{CG}\right)}{v_T} \tag{3.4-2}$$

Figure 3-13 shows that the induced angle-of-attack has a sign that is opposite the sign of the rocket body angle-of-attack that caused the rotation.

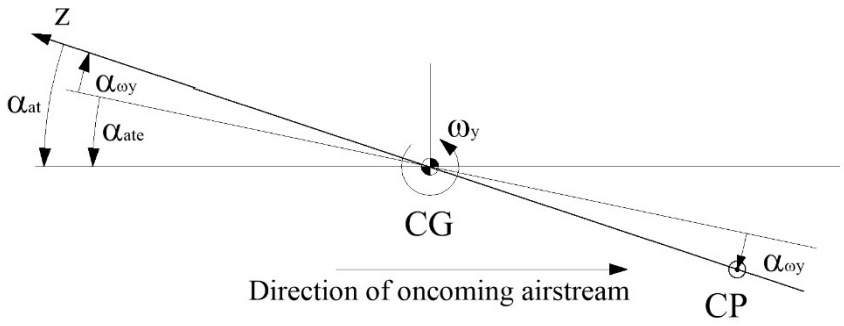

Figure 3-13 Net angle-of-attack due to rocket's rotation

The induced angle-of-attack creates a normal force on the rocket that is proportional to the rotation rate of the rocket. And the sign of the induced angle-of-attack is such that that normal force pushes back on the rotation of the rocket in the direction in which it is rotating. The greater rotation rate of the rocket, the greater the normal force pushing back on this rotation, which acts to dampen the rotation of the rocket, making it a damping normal force. The effect of the induced angle-of-attack is to decrease the total net or effective angle-of-attack.

Note that this calculation of the induced angle-of-attack assumes that the rotational velocity is a constant value over the chord of the fin, which is the method used by Barrowman. This approximation is valid when the distance from the center of gravity of the rocket to the center of pressure of the fin is large compared to the root chord length of the fin so that the variation in the angle-of-attack is small along the length of the fin chord. A more accurate result would be obtained using strip theory to calculate the damping force and moment using the actual tangential velocity and induced angle-of-attack at each point along the chord. This is the method used to calculate the roll induced angle-of-attack and the roll damping normal force and moment in Section 3.10. Applying this method to pitch damping is left as a topic for future exploration.

3.5 Total Angle-of-Attack for Pitch & Yaw Rotations

The total angle-of-attack for the fins for pitch and yaw rotations is comprised of three components, the angle-of-attack of the rocket body to the direction of the oncoming airstream, the induced angle-of-attack due to the pitch and yaw rotations of the rocket, and the rotational angle of the fins.

Figure 3-14 shows that when the rocket is at an angle-of-attack to the oncoming airstream, there is a normal force that generates a yaw or pitch moment about the x or y-axes. Pitch and yaw control is usually done using 4 fins or canards so that two of the opposing fins work together to control pitch, and the other two opposing fins work to control yaw. Opposite fins are rotated in the same rotational direction about the x or y-axis in the rocket frame of reference axis system to control yaw and pitch.

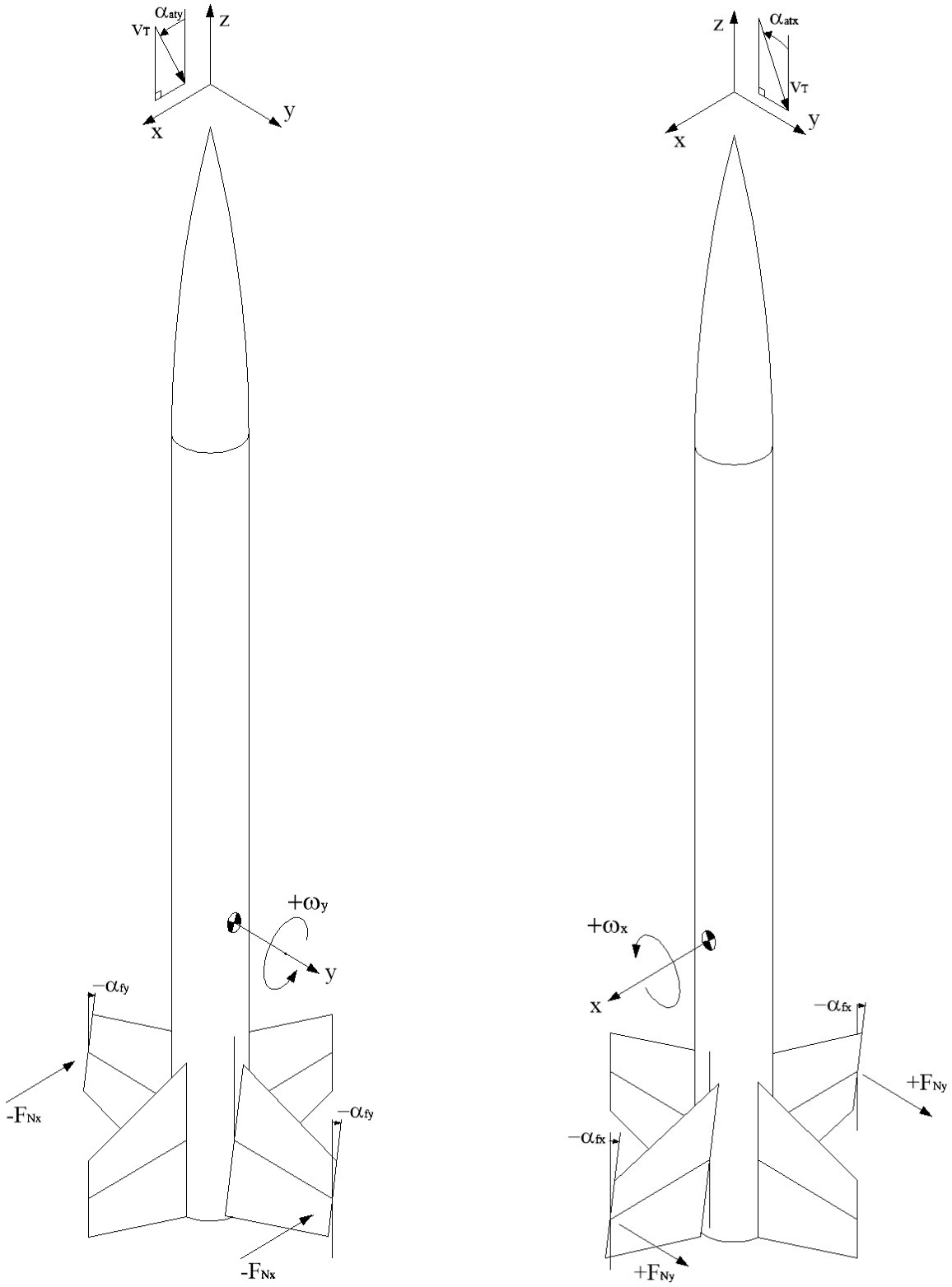

Pitch Yaw

Figure 3-14 Pitch and Yaw Rotations

Using the rocket frame of reference axis convention shown in Figure 2-6, Figure 3-15 shows that both a positive pitch angle-of-attack, the sign of the angle-of-attack is the sign of a rotation from the z-axis of the rocket to the oncoming airstream vector, and a negative rotation angle of the fin both produce a negative normal force on the fin. That negative normal force, in turn, creates a positive rotational moment about the rocket's center of gravity if the fins are behind the center of gravity. If the fins were in front of the center of gravity, the normal force would still be negative, but the moment and rotation would then be in a negative direction about the center of gravity.

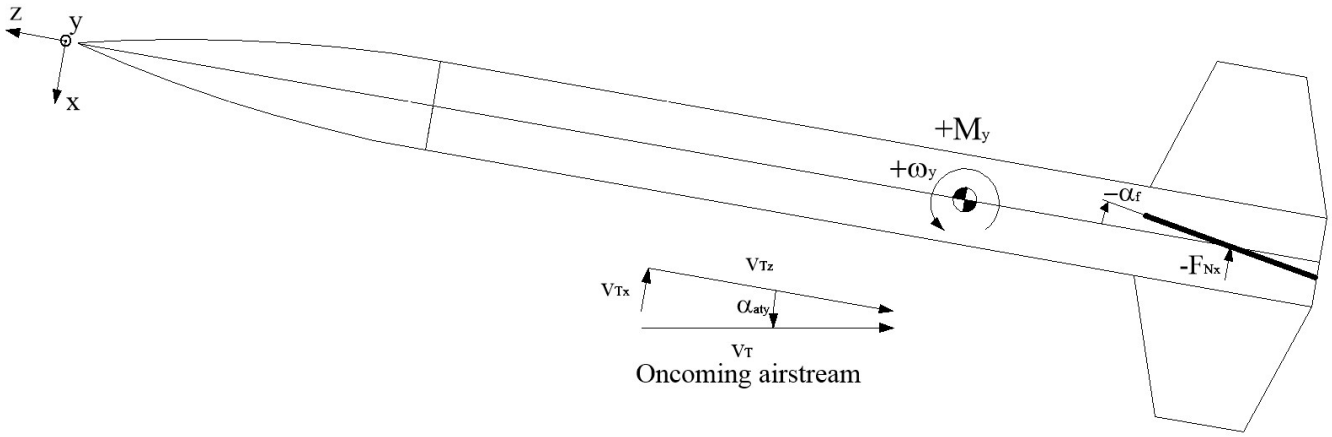

Figure 3-15 Pitch angle-of-attack and fin rotation angle

Figure 3-17 shows that both a positive yaw angle-of-attack and a negative rotation angle of the fin both produce a positive normal force on the fin in the rocket frame of reference, the opposite sign of the pitch normal force. That positive normal force, in turn, creates a positive rotational moment about the rocket's center of gravity if the fins are behind the center of gravity. If the fins were in front of the center of gravity, the normal force would still be negative, but the moment and rotation would then be in a negative direction about the center of gravity.

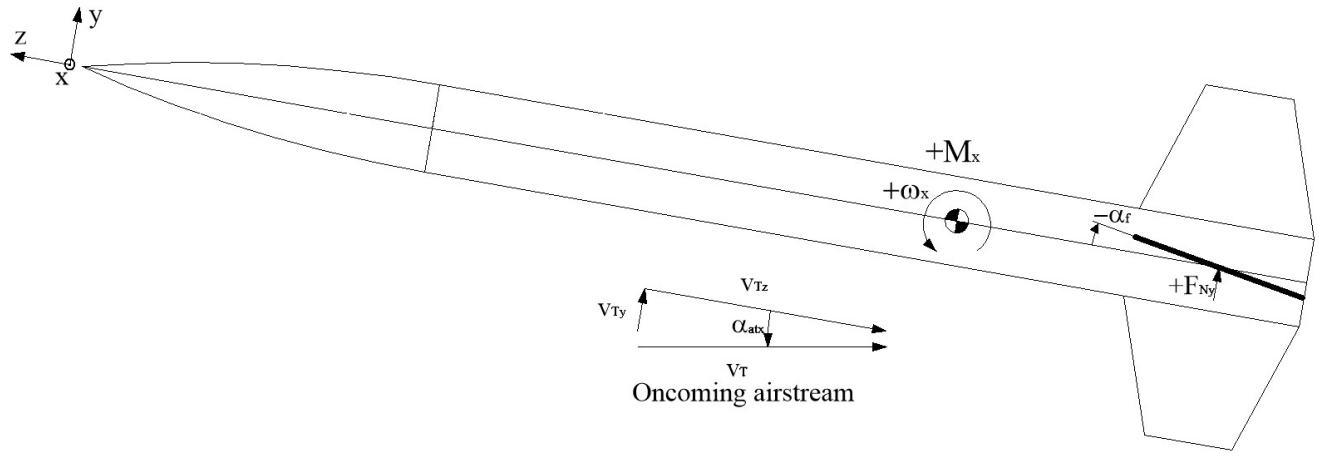

Figure 3-16 Yaw angle-of-attack and fin rotation angle

The three components of the total pitch and yaw angles-of-attack, the body angle-of-attack, the induced angle-of-attack, and the angle of the fins, can be combined into one total angle-of-attack that can be used to calculate the total normal force on the fins and the total rotational moment created by that normal force. When adding these three components, the sign for each compound is determined by the sign of the effect it has on the normal force.

Since the pitch and yaw rotation are orthogonal, each will have its own body angle-of-attack. That angle-of-attack will be the angle between the z-axis of the rocket and the oncoming airstream in the x-z plane as shown in Figure 3-15 for pitch and in the y-z plane as shown in Figure 3-16 for yaw.

To start, the body angle-of-attack will be assumed to be positive, and the signs of the induced angle-of-attack and fin angle will be set by the relative impact on the normal forces they create. Section 3.4 showed that the normal force created by the pitch induced angle-of-attack pushes back on the normal force that caused the rotation, so the sign of the pitch induced angle-of-attack is the opposite of the pitch angle-of-attack. The same is true for the yaw induced angle-of-attack. And in Figure 3-15 and Figure 3-16, it was shown that a fin rotation angle opposite the sign of the angle-of-attack of the body produces a normal force of the same sign as the body angle-of-attack, so the sign of the contribution of the fin rotation angle will also be the opposite of the pitch and yaw angles-of-attack.

Now that the relative signs have been determined, the last step is to add the interference factors. The tail-body interference factor described in Section 3.2 modifies the body angle-of-attack. This factor accounts for the increased airflow around the rocket when the body is at an angle-of-attack to the oncoming airstream, per equation (3.2-1). The tail-body interference factor due to the angle of the fin relative to the body tube applies to the angle between the body and the fin, although this interference factor was shown to be negligible and can be ignored in most cases.

There is no interference factor for the induced angle-of-attack because the induced angle-of-attack is due solely to the net airstream due to the rocket's rotation rate.

The total angle-of-attack for the fins, including the tail-body interference factors for pitch

$$\alpha_{atey} = K_{TBf} \cdot \alpha_{at} - k_{TBf} \cdot \alpha_{fy} - \frac{\omega_y \cdot \left(L_{CPf} - L_{CG} \right)}{V_T} \tag{3.5-1}$$

and yaw

$$\alpha_{atex} = K_{TBf} \cdot \alpha_{at} - k_{TBf} \cdot \alpha_{fx} - \frac{\omega_x \cdot \left(L_{CPf} - L_{CG} \right)}{V_T} \tag{3.5-2}$$

3.6 Pitch and Yaw Forcing and Damping Normal Forces and Moments

Using the total angle-of-attack equation (3.5-1), and the sign of the pitch normal force from Figure 3-15, the total pitch normal force is given by

$$F_{Nx} = -\frac{\rho}{2} \cdot A_r \cdot {v_T}^2 \cdot C_{N\alpha} \cdot \left(K_{TBf} \cdot \alpha_{aty} - k_{TBf} \cdot \alpha_{fy} - \frac{\omega_y \cdot \left(L_{CPf} - L_{CG} \right)}{V_T} \right) \tag{3.6-1}$$

Using the sign of the yaw normal force form Figure 3-16, the total yaw normal force is

$$F_{Ny} = \frac{\rho}{2} \cdot A_r \cdot {v_T}^2 \cdot C_{N\alpha} \cdot \left(K_{TBf} \cdot \alpha_{atx} - k_{TBf} \cdot \alpha_{fx} - \frac{\omega_x \cdot \left(L_{CPf} - L_{CG} \right)}{V_T} \right) \tag{3.6-2}$$

Breaking out the forcing, F_{N1}, and damping, F_{N2}, components of the normal force separately, for pitch

$$F_{N1xf} = -\frac{\rho}{2} \cdot A_r \cdot {v_T}^2 \cdot C_{N\alpha T} \cdot \left(K_{TB} \cdot \alpha_{aty} - k_{TB} \cdot \alpha_{fy} \right) \tag{3.6-3}$$

$$F_{N2xf} = \frac{\rho}{2} \cdot A_r \cdot \left| v_T \right| \cdot C_{N\alpha T} \cdot \omega_y \cdot \left(L_{CPf} - L_{CG} \right) \tag{3.6-4}$$

and for yaw

$$F_{N1yf} = \frac{\rho}{2} \cdot A_r \cdot {v_T}^2 \cdot C_{N\alpha T} \cdot \left(K_{TB} \cdot \alpha_{atx} - k_{TB} \cdot \alpha_{fx} \right) \tag{3.6-5}$$

$$F_{N2yf} = -\frac{\rho}{2} \cdot A_r \cdot |v_T| \cdot C_{N\alpha T} \cdot \omega_x \cdot \left(L_{CPf} - L_{CG} \right) \tag{3.6-6}$$

For the pitch normal force, v_T is the positive magnitude of the total airstream velocity passing over the rocket due to the lateral wind and the forward velocity of the rocket. The sign of the normal force is then set assuming the airstream velocity is a positive magnitude so that the force has the correct directional orientation.

Using the sign of the pitch normal force and resulting rotational moment from Figure 3-15, the pitch rotational moment is given by

$$M_{yf} = -F_{Nxf} \cdot \left(L_{CPf} - L_{CG} \right) \tag{3.6-7}$$

and using the sign of the yaw normal force and resulting rotational moment from Figure 3-16, the yaw rotational moment is given by

$$M_{xf} = F_{Nyf} \cdot \left(L_{CPf} - L_{CG} \right) \tag{3.6-8}$$

Breaking out the forcing, M_1, and damping, M_2, components of the normal force separately, for pitch

$$M_{1yf} = \frac{\rho}{2} \cdot A_r \cdot {v_T}^2 \cdot \left(L_{CPf} - L_{CG} \right) \cdot C_{N\alpha T} \cdot \left(K_{TB} \cdot \alpha_{aty} - k_{TB} \cdot \alpha_{fy} \right) \tag{3.6-9}$$

$$M_{2yf} = -\frac{\rho}{2} \cdot A_r \cdot |v_T| \cdot \left(L_{CPf} - L_{CG} \right)^2 \cdot C_{N\alpha T} \cdot \omega_y \tag{3.6-10}$$

and for yaw

$$M_{1xf} = \frac{\rho}{2} \cdot A_r \cdot {v_T}^2 \cdot \left(L_{CPf} - L_{CG} \right) \cdot C_{N\alpha T} \cdot \left(K_{TB} \cdot \alpha_{atx} - k_{TB} \cdot \alpha_{fx} \right) \tag{3.6-11}$$

$$M_{2xf} = -\frac{\rho}{2} \cdot A_r \cdot |v_T| \cdot \left(L_{CPf} - L_{CG} \right)^2 \cdot C_{N\alpha T} \cdot \omega_x \tag{3.6-12}$$

where L_{CPf} is the center of pressure of the fin measured from the tip of the nosecone. M_{1f} is the forcing moment that includes the moment that is generated by the angle of the fin and the moment that is generated by the body angle-of-attack that aligns the rocket with the oncoming airstream. M_{2f} is the damping moment which serves to dampen the rotation of the rocket by pushing back in the direction of rotation. The pitch and yaw normal forces have opposite signs in the rocket axis system, but the moments have the same signs relative to the signs of the angles-of-attack.

If the fin or canard control surfaces are ahead of the center of gravity rotation point, the sign of the normal force stays the same, but the sign of the rotational moment reverses because the normal force is applied to the other side of

the center of gravity. This is taken care of automatically by equations (3.6-9) to (3.6-12) because the fin's center of pressure location, L_{CPf}, goes from a number greater than the length of the center of gravity, L_{CG}, to a number that is less than the length of the center of gravity, reversing the sign of the moment..

If the moments are being calculated for each fin individually, then the value for the normal force coefficient derivative in equations (3.6-3) , (3.6-4), (3.6-9), and (3.6-10) would be the normal forced coefficient derivative for a single fin, $C_{N\alpha 1}$, from equation (3.1-3). But if opposite fins are being controlled together, then the normal force coefficient derivative for the complete tail $C_{N\alpha T}$, from equation (3.1-10), where 2 of the 4 fins are contributing, would be used.

These are the aerodynamic parameters just for the fins. The process for combining the fin aerodynamic parameters, where fins are used as pitch control surfaces, with the aerodynamic parameters for the other rocket components will be covered in the paper on *Pitch and Roll Dynamics Modeling.*

3.7 Roll Induced Angle-of-Attack

Like the induced angle-of-attack due to a pitch rotation, there is an induced angle-of-attack due to a roll rotation. Figure 3-17 shows the induced angle-of-attack, $\alpha_{\omega z}$, due to the roll. The roll induced angle-of-attack is a function of the distance from the longitudinal center line of the rocket as the radial velocity of the fin increases at greater radial distance from the center. Unlike the pitch induced angle-of-attack, which was approximated to be constant across the length of the fin, the roll induced angle-of-attack varies significantly across the span of the fin, so that variation must be considered when calculating the roll normal force.

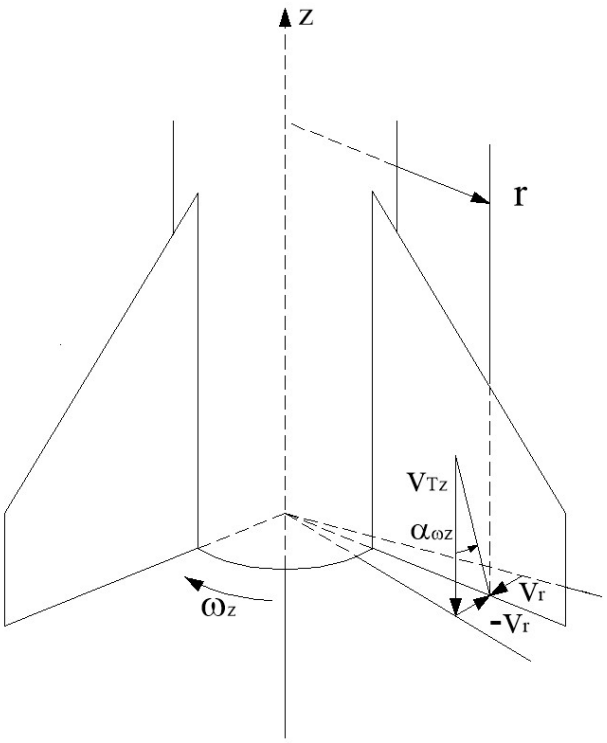

Figure 3-17 Roll induced angle-of-attack

The radial tangential velocity of the fin due to the roll rotation is

$$v_r = \omega_z \cdot r \tag{3.7-1}$$

The induced wind velocity is opposite the rotation velocity, or $-v_r$, and the induced angle-of-attack is

$$\alpha_{\omega z} = \arctan\frac{-v_r}{v_{Tz}} \simeq \frac{-\omega_z \cdot r}{v_{Tz}} \tag{3.7-2}$$

where v_{Tz} is the z-axis velocity of the oncoming airstream.

Like the pitch induced angle-of-attack, the roll induced angle-of-attack creates a normal force on the rocket that is proportional to the rotation rate of the rocket, and the sign of the roll induced angle-of-attack is such that that normal force pushes back opposite the direction in which it is rolling. The greater roll rate of the rocket, the greater the normal force pushing back on this rotation, which acts to dampen the rotation of the rocket, making it a damping normal force.

3.8 Roll Damping Tail-body Interference

In section 3.42 of his thesis[34], Barrowman derives the roll damping interference factor. This interference factor is based on the same crossflow that occurs when the body is at a non-zero angle-of-attack, described in Section 3.2 of this paper. The interference factor is caused by an increased velocity of the airstream as it passes around the body, as described in equation (3.2-1) and shown in Figure 3-8.

When this velocity profile is applied to the roll induced angle-of-attack from equation (3.7-2), Barrowman gives the effective angle-of-attack with the tail-body interference as[35]

$$\alpha_{\omega zi} = -\frac{\omega_z}{v_T} \cdot \left(r + \frac{r_t^3}{r^2} \right) \tag{3.8-1}$$

The induced angle-of-attack without the tail-body interference from equation (3.7-2) is

$$\alpha_{\omega z} = -\frac{\omega_z \cdot r}{v_T} \tag{3.8-2}$$

where the velocity of the airstream orthogonal to the fins due to the z-axis rotation of the rocket is

$$v = -\omega_z \cdot r \tag{3.8-3}$$

The equivalent orthogonal airstream velocity for the modified angle-of-attack in equation (3.8-1) is

$$v' = -\omega_z \cdot \left(r + \frac{r_t^3}{r^2} \right) \tag{3.8-4}$$

Figure 3-18 shows the orthogonal induced velocities with and without the tail-body interference normalized to the roll rate and the radius away from the body tube. The graph shows that, at the radius of the body tube, the orthogonal rotational velocity is $\omega_z \cdot r_t$, and that the velocity with the tail-body interference would be twice that velocity. At larger radii, the velocities converge.

---

[34] (Barrowman J. S., 1967, p. 41)

[35] (Barrowman J. S., 1967, pp. 41 eq (3-119))

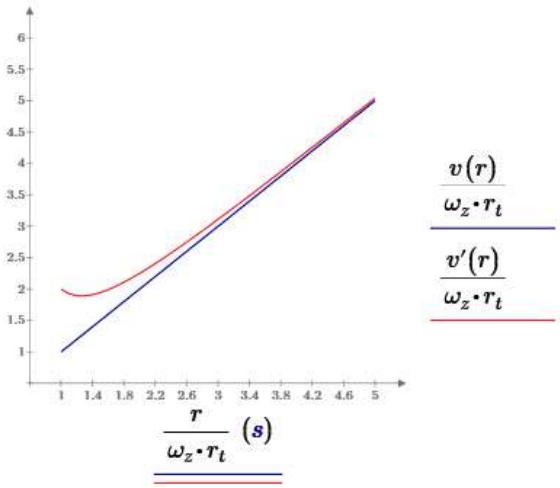

Figure 3-18 Normalized orthogonal velocities with and without the tail-body interference

But there is no physical mechanism that would cause the velocity of the effective orthogonal airstream to rotate at twice the rotation rate of the rocket at the boundary of the body tube, all the way around the circumference of the body tube. In the case of a rotating tube, if the body is at a physical angle-of-attack, the velocity of the orthogonal airstream would be modified by the airflow around the body as described in Section 3.2. On one side of the body, the modified airflow over the fin would add to the roll induced airflow, but, for the opposite fin, the modified airflow would reduce the net airflow because that fin's tangential velocity is in the opposite direction, so the net impact of the airflow around the body would be zero. For a single fin, the impact of the airflow around the body would be sinusoidal as the fin rolls around the body but net out to zero over a complete 360 degree rotation.

The tail-body interference is fully accounted for by multiplying the body angle-of-attack by the tail-body interference factor. The tail-body interference does not affect the roll induced angle-of-attack, and therefore, a roll damping tail-body interference factor is not needed[36].

3.9 Total Angle-of-Attack for Roll Rotation

Figure 3-14 showed that when the rocket is at a pitch or yaw angle-of-attack to the oncoming airstream, there is a normal force that generates a moment about the x or y-axes, but there is no roll moment generated about the z-axis because the normal forces on either side of the longitudinal centerline of the rocket are equal. It takes an imbalanced

[36] James Barrowman agreed with this conclusion in an email exchanged with the author in September 2025

angle-of-attack to generate roll which does not happen as a result to the rocket being at an angle-of-attack to the oncoming airstream. Roll can be caused by one or more of the fins being at an angle to the longitudinal z-axis of the rocket, by another airframe asymmetry, or it can be caused by thrust imbalance in the motor.

Figure 3-19 shows the case where there are equal and opposite normal forces on the fins on opposite sides of the rocket's center line due to the angles of the fins, resulting in a roll moment. If the normal force on each of the opposite fins are equal and opposite, there is no pitch or yaw moment because there is not a net x or y-axis normal force. If the normal forces of the opposing fins are not equal, there will be both a roll moment and a pitch and or yaw moment generated.

For 4 fins being used to induce or control roll, opposite fins are rotated in opposite angles along the axes of the rocket frame of reference as shown in Figure 3-19. In this figure, the fin aligned with the positive y-axis has a positive rotation and produces a normal force aligned with the positive x-axis. The fin aligned with the negative y-axis has a negative rotation and produces a normal force aligned with the negative x-axis. But both fins produce a negative moment and roll about the rocket's z-axis. The same is true for the fins aligned with the x-axis.

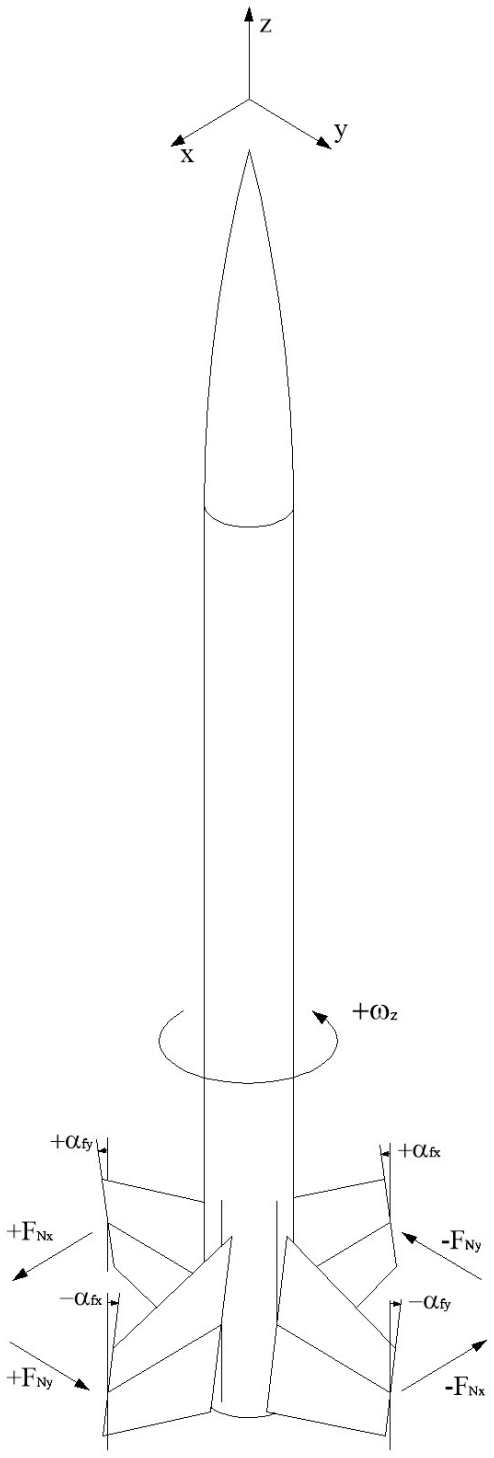

Figure 3-19 Normal force symmetry resulting in a roll rotation from above

Figure 3-20 shows that a fin that is aligned with the positive y-axis (the bottom right hand fin in Figure 3-19 that is coming out of the page in Figure 3-20), canted in a negative angular rotation about the y-axis creates a normal force

in the direction of the negative x-axis, resulting in a positive moment and roll about the rocket's z-axis. When opposite fins are canted in opposite rotational directions as shown in Figure 3-19, opposite fins have opposite signs for their normal forces, but all four fins contribute constructively with the same sign to the total moment about the z-axis.

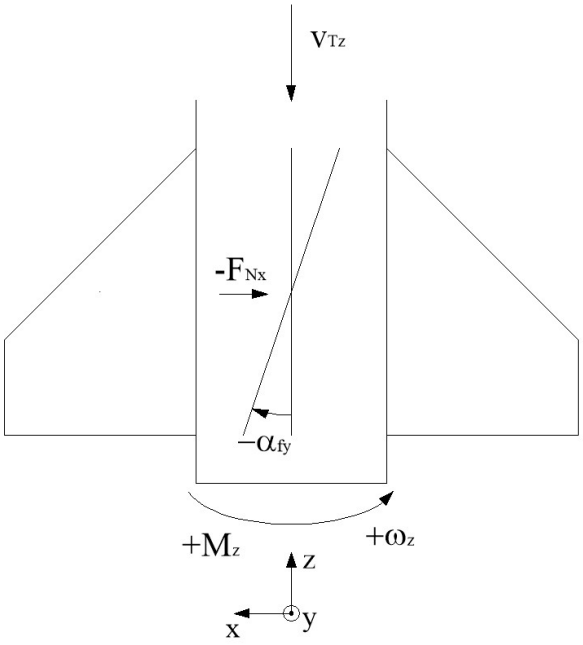

Figure 3-20 Canted fin and resulting normal force, rotational moment, and rotation direction for the fin aligned with the positive y-axis

Since neither the pitch nor yaw angle-of-attack induces roll, the total angle-of-attack for a roll rotation is comprised of two components, the rotational angle of the fins, and the induced angle-of-attack due to the roll rotation of the rocket.

The induced angle-of-attack produces a normal force that pushes back on the direction in which the rocket is rolling. So, from Figure 3-20, a negative rotation rate will produce a normal force in the negative x-axis direction, which produces a positive moment about the z-axis, so the induced angle-of-attack component is also negative.

The tail-body interference factor due to the rotation angle of the fin, described in Section 3.3, modifies the effective rotation angle of the fin. Again, this interference factor was shown to be negligible and can be ignored in most cases. There is no interference factor for the induced angle-of-attack because the induced angle-of-attack is due solely to the net airstream due to the rocket's roll rate and the z-axis airstream velocity.

The total angle-of-attack of the fins, including the tail-body interference factors is

$$\alpha_{ats} = -k_{TBf} \cdot \alpha_f - \frac{\omega_z \cdot r}{v_{Tz}} \tag{3.9-1}$$

3.10 Roll Forcing and Damping Normal Forces and Moments

Since the roll angle-of-attack for equation (3.9-1) is a function of the distance from the longitudinal centerline of the rocket, or radius r, the normal force will also be a function of the radius. The total force on the fins is determined using strip theory (see Section 2.7). The fin is broken up into a number of incremental strips as shown in Figure 3-21, and the force on each individual strip is calculated using the angle-of-attack at that radius from equation (3.9-1). The portion of the force in that strip is the total force on the fin at that strip's angle-of-attack times the area of the strip divided by the total area of the fin. The incremental normal force in any strip, then, is

$$dF_{Nz} = \frac{\rho}{2} \cdot A_r \cdot {v_{Tz}}^2 \cdot C_{N\alpha R} \cdot \alpha_{ats}(r) \cdot \frac{c(r) \cdot dr}{A_f} \tag{3.10-1}$$

where $c(r)$ is the chord for the fin at radius r, and is defined by equation (2.6-6).

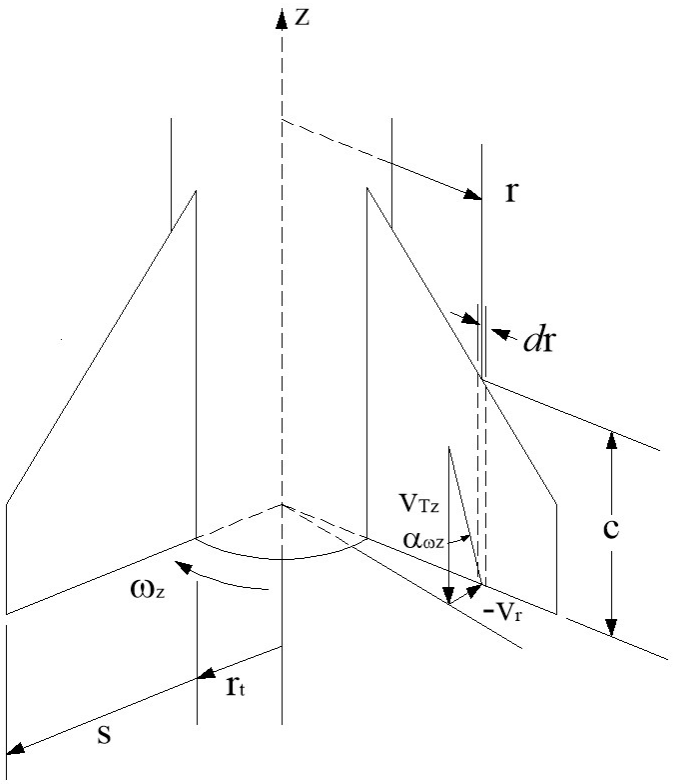

Figure 3-21 Calculating the incremental force on a vertical strip of the fin

The angle-of-attack is defined by equation (3.9-1) and consists of two parts. The portion of the roll angle-of-attack due to the angle of the fins creates the forcing normal force, and the portion due to the induced angle-of-attack gives rise to the damping normal force. Combining the total roll angle-of-attack from equation (3.9-1) with equation (3.10-1), and breaking out the forcing, dF_{N1x} , and damping, dF_{N2z} , components of the normal force separately

$$dF_{N1z} = -\frac{\rho}{2} \cdot A_r \cdot {v_{Tz}}^2 \cdot C_{N\alpha R} \cdot \alpha_f \cdot \frac{c(r) \cdot dr}{A_f} \tag{3.10-2}$$

$$dF_{N2z} = -\frac{\rho}{2} \cdot A_r \cdot |v_{Tz}| \cdot C_{N\alpha R} \cdot \omega_z \cdot r \cdot \frac{c(r) \cdot dr}{A_f} \tag{3.10-3}$$

v_{Tz} is the z-axis component of the total airstream velocity in the rocket frame of reference. It is only the z-axis component of the total airstream vector that causes the roll of the rocket. The z-axis component of the total airstream velocity has a sign, but to be consistent with the total airstream velocity used for pitch, the magnitude of v_{Tz} is used in the roll damping moment, and the sign of the moment is then set to ensure it has the correct rotational direction.

To calculate the resulting incremental moment, the incremental normal force is multiplied by the radius of the incremental strip

$$dM_z = dF_{nz} \cdot r \tag{3.10-4}$$

and to find the total roll moment, the incremental moment is integrated across the span of the fin

$$M_z = \int_{r_t}^{s+r_t} dF_N \cdot r \cdot dr \tag{3.10-5}$$

Combining equations (3.10-2) and (3.10-5), the total roll forcing moment is

$$M_{1zf} = -\frac{\rho}{2} \cdot A_r \cdot {v_{Tz}}^2 \cdot C_{N\alpha R} \cdot \frac{\int_{r_t}^{s+r_t} c(r) \cdot r \cdot dr}{A_f} \cdot \alpha_f \tag{3.10-6}$$

Since the area of the fin from equation (2.6-7) is

$$A_f = \int_{r_t}^{s+r_t} c(r) \cdot dr \tag{3.10-7}$$

equation (3.10-6) can be written as

$$CA_{Rf} = \frac{\int_{r_t}^{s+r_t} c(r) \cdot r \cdot dr}{\int_{r_t}^{s+r_t} c(r) \cdot dr} \tag{3.10-8}$$

that has the form of the center of a distribution, which, in this case, is recognizable as the radial center of area, with units of length.

CA_{Rf} is the distance from the z-axis centerline of the rocket to the center of area of the fin. Written in terms of the center of area, the roll forcing moment is

$$M_{1zf} = -\frac{\rho}{2} \cdot A_r \cdot v_{Tz}{}^2 \cdot CA_{Rf} \cdot C_{N\alpha R} \cdot \alpha_f \tag{3.10-9}$$

which agrees with Barrowman[37]. The radial center of area, CA_{Rf}, is the moment arm length of the radial forcing moment for the application of the forcing normal force, corresponding to $\left(L_{CP} - L_{CG}\right)$ in the pitch forcing moment equation. This is to say that

$$M_{1zf} = F_{N1zf} \cdot CA_{Rf} \tag{3.10-10}$$

If the roll moment for a single fin is being calculated, then $C_{N\alpha 1}$ would be used rather than $C_{N\alpha R}$.

The tail-body interference factor due to the rotation angle of the fin described in Section 3.3 modifies the angle-of-attack for both pitch and roll. The forcing moment with the tail-body interference factor is

$$M_{1zf} = -\frac{\rho}{2} \cdot A_r \cdot v_{Tz}{}^2 \cdot CA_{Rf} \cdot C_{N\alpha Rf} \cdot k_{TBf} \cdot \alpha_f \tag{3.10-11}$$

For the contribution of each of the fins to the total roll rotational moment, equation (3.10-11) assumes the sign of the fin rotation direction applies to the fins aligned with the positive x and y-axes, and assumes that the rotation angle for the fins aligned with the negative x and y-axes is opposite the rotation angle of the fins aligned with the positive axes as shown in Figure 3-19.

Using Mathcad to solve for the center of area symbolically

$$CA_{Rf} = \frac{\int_{r_t}^{s+r_t} c(r) \cdot r \cdot dr}{\int_{r_t}^{s+r_t} c(r) \cdot dr} = \frac{s}{3} \cdot \frac{2 \cdot c_t + c_r}{c_t + c_r} + r_t \tag{3.10-12}$$

which is the same result Barrowman gives for the radial center of pressure[38].

For the roll damping moment, combining equations (3.10-3) and (3.10-5), the total roll damping moment is

---

[37] (Barrowman J. S., 1967, pp. 11 eq (3-31)) Barrowman calls this term the radial center of pressure, which is derived from the mean chord, but does not make the connection with it also being the center of area of the fin

[38] (Barrowman J. S., 1967, p. 10 eq. 3.27)

$$M_{2zf} = -\frac{\rho}{2} \cdot A_r \cdot \left| v_{Tz} \right| \cdot C_{N\alpha Rf} \cdot \frac{\int_{r_t}^{s+r_t} c(r) \cdot r^2 \cdot dr}{A_f} \cdot \omega_z \tag{3.10-13}$$

The integral in the numerator of the roll damping moment has two factors of r, one from the induced angle-of-attack, and the other from the moment arm. Defining CM_{Rf} as

$$CM_{Rf} = \sqrt{\frac{\int_{r_t}^{s+r_t} c(r) \cdot r^2 \cdot dr}{\int_{r_t}^{s+r_t} c(r) \cdot dr}} \tag{3.10-14}$$

where the integral in the denominator is the area of the fin, then the roll damping moment becomes

$$M_{2zf} = -\frac{\rho}{2} \cdot A_r \cdot \left| v_{Tz} \right| \cdot {CM_{Rf}}^2 \cdot C_{N\alpha Rf} \cdot \omega_z \tag{3.10-15}$$

As shown in Section 3.8, there is no interference factor for the induced angle-of-attack.

Using Mathcad to solve for CM_R symbolically

$$CM_{Rf} = \sqrt{\frac{\int_{r_t}^{s+r_t} c(r) \cdot r^2 \cdot dr}{\int_{r_t}^{s+r_t} c(r) \cdot dr}} = \sqrt{\frac{\left(3 \cdot c_t + c_r\right) \cdot s^2 + \left(8 \cdot c_t + 4 \cdot c_r\right) \cdot r_t \cdot s + \left(6 \cdot c_t + 6 \cdot c_r\right) \cdot {r_t}^2}{6 \cdot \left(c_t + c_r\right)}} \tag{3.10-16}$$

This can also be expressed in terms of λ, τ, and r_t

$$CM_{Rf} = \sqrt{\frac{\left(\left(3 \cdot \lambda + 1\right) \cdot s^2 + 4 \cdot \left(2 \cdot \lambda + 1\right) \cdot s \cdot r_t + 6 \cdot \left(\lambda + 1\right) \cdot {r_t}^2\right)}{6 \cdot \left(\lambda + 1\right)}} \tag{3.10-17}$$

CM_R has units of length and has the form of an engineering quantity called the radius of gyration[39]. In one of its forms, the radius of gyration is the root mean square of the second moment of area over the total area, which matches the form of equation (3.10-14). In this case, the radius of gyration represents the effective moment arm length for the application of the damping normal force to create the damping moment. $CM_{Rf}{}^2$ corresponds to the $\left(L_{CPf} - L_{CG}\right)^2$ term in the pitch damping moment in equation (3.6-10), much like the radial center of area, CA_{Rf}, is the moment arm for the radial forcing moment.

Evaluating the expressions for the radial center of area and radius of gyration for test rocket VTS-1, $CA_{Rf} = 3.34in$ and $CM_{Rf} = 3.527in$. For pitch, the moment arms for the forcing and damping moments are the same, but for roll, the two moment arms are a little different.

Barrowman analyzes the roll damping with $C_{N\alpha R}$ and $CM_R{}^2$ combined into a single term[40], C_{lp}, where

$$C_{lp} = \frac{c_r \cdot s}{6 \cdot L_r{}^2} \cdot \left(\left(1 + 3 \cdot \lambda\right) \cdot s^2 + 4 \cdot \left(1 + 2 \cdot \lambda\right) \cdot s \cdot r_t + 6 \cdot \left(1 + \lambda\right) \cdot r_t^2 \right) \cdot N \cdot C_{N\alpha 1} \tag{3.10-18}$$

so Barrowman's equivalent to the radius of gyration is

$$CM_{Rf} = \sqrt{\frac{c_r \cdot s}{6 \cdot L_r{}^2} \cdot \left(\left(1 + 3 \cdot \lambda\right) \cdot s^2 + 4 \cdot \left(1 + 2 \cdot \lambda\right) \cdot s \cdot r_t + 6 \cdot \left(1 + \lambda\right) \cdot r_t^2 \right)} \tag{3.10-19}$$

Equation (3.10-19) includes the variable L_r, which Barrowman defines as a reference length, but nowhere is it related to a physical parameter of the rocket. If the assumption is made that $L_r{}^2 = A_f$, the area of a fin, then it can be shown that equation (3.10-19) equals equation (3.10-17), so the calculation of the radial damping moment is in agreement.

3.11 Fin Center of Pressure

[39] (Radius of gyration, 2025)

[40] (Barrowman J. S., 1967, p. 17 eq. 3.51)

There is both a radial and longitudinal component to the center of pressure of a fin. For a thin airfoil, the longitudinal center of pressure is located along the ¼ chord line[41]. Radially, the center of pressure is located at the radial center of area, as shown above. Where these two lines intersect is the center of pressure of the fin as shown in Figure 3-22.

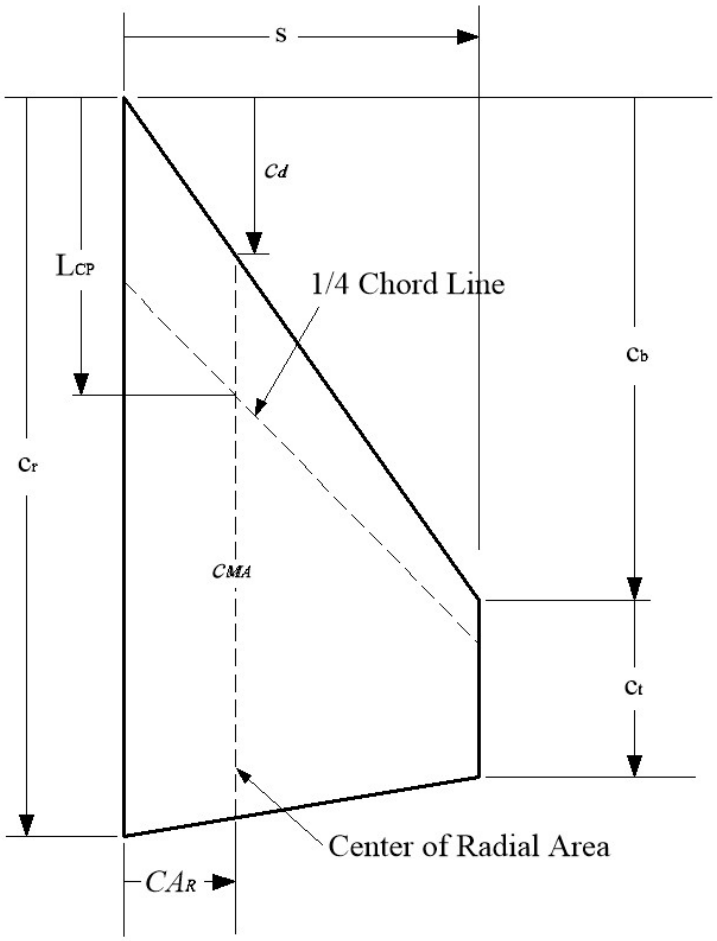

Figure 3-22 Finding the center of pressure of a fin at the intersection of the ¼ chord line and the radial center of area

It was shown in equation (3.10-12) that the radial center of pressure for a fin is the radial center of area, which is given by

[41] (Barrowman J. S., 1967, pp. 6-7)

$$CA_{Rf} = \frac{\int_{r_t}^{s+r_t} c(r) \cdot r \cdot dr}{\int_{r_t}^{s+r_t} c(r) \cdot dr} = \frac{1}{3} \cdot s \cdot \frac{2 \cdot c_t + c_r}{c_t + c_r} \tag{3.11-1}$$

The length of the chord at the center of radial area, also the mean chord line, from equation (2.6-6) is

$$c_{MA} = \frac{CA_{Rf} \cdot \left(c_c - c_b\right)}{s} + c_r \tag{3.11-2}$$

The distance from the tip of the root edge to the mean chord line is

$$c_d = \frac{c_b}{s} \cdot CA_R \tag{3.11-3}$$

so the longitudinal center of pressure is ¼ the mean chord line plus the distance from the tip of the leading edge of the fin to the start of the mean chord line

$$L_{CPf} = \frac{c_b}{s} \cdot CA_R + \frac{c_{MA}}{4} = \frac{c_b}{3} \cdot \left(\frac{c_r + 2 \cdot c_t}{c_r + c_t} \right) + \frac{1}{6} \cdot \left(c_r + c_t - \frac{c_r \cdot c_t}{c_r + c_t} \right) \tag{3.11-4}$$

which is the same result as Barrowman[42]

The tail-body interference factor also applies to the radial center of pressure because it increases the effective angle-of-attack for offsets closer to the body. Barrowman[43] cites Pitts, Nielsen, & Kaattari[44] as determining that the longitudinal center-of-pressure is independent of the interference flow, but the impact can be quantified.

The center of area with the tail-body interference is the center of area equation (3.11-1) with the addition of the angle-of-attack interference factor due to the tail-body interference from equation (3.2-3). This is the radially weighted force on each strip divided by the total force, both including the angle-of-attack interference factor, which is

---

[42] (Barrowman J. S., 1967, pp. 10 eq, (3-30))

[43] (Barrowman J. S., 1967, p. 31 Section 3.31)

[44] (Pitts, Neilsen, & Kaattari, 1957, p. 581)

$$CA_{RTB} = \frac{\int_{r_t}^{(r_t+s)} c(r)\cdot r\cdot\left(1+\frac{r_t^2}{r^2}\right)\cdot dr}{\int_{r_t}^{r(_t+s)} c(r)\cdot\left(1+\frac{r_t^2}{r^2}\right)\cdot dr} \tag{3.11-5}$$

Note that this change in the radial center of pressure applies only to a pitch rotation and not a roll rotation. For roll, the symmetry of the increased flow over the fins would cancel the net effect on the fins, so this only applies to calculating the intersection of the radial center of pressure and the ¼ chord line to calculate the center of pressure.

The radial center of pressure interference factor, then, is the radial center of area with the interference divided by the radial center of area without the interference

$$k_{TBCAR} = \frac{CA_{RTB}}{CA_R} \tag{3.11-6}$$

Using Mathcad to solve this in terms of τ and λ

$$k_{TBCAR} = \left[\frac{2\cdot(\lambda+1)\cdot(\tau-1)\cdot\left(\left(\lambda^2-2\cdot\lambda-2\right)\cdot\tau^2+\left(2\cdot\lambda^2+2\cdot\lambda-4\right)\cdot\tau+3\cdot\lambda^2\right)}{(\lambda-1)\cdot(2\cdot\lambda+1)\cdot\left((2\cdot\lambda+1)\cdot\tau\cdot\ln(\tau)+(\lambda+1)\cdot\tau^3-2\cdot\lambda\cdot\tau^2-(\lambda+1)\cdot\tau+2\cdot\lambda\right)}+\frac{3\cdot(\lambda+1)\cdot(\tau+(1-2\cdot\lambda))}{(\lambda-1)\cdot(2\cdot\lambda+1)\cdot(\tau-1)}\right] \tag{3.11-7}$$

The longitudinal center of pressure is determined by the intersection of the ¼ chord line and the radial center of pressure. The center of pressure's falling along the ¼ chord line does not change due to the tail-body interference because the angle-of-attack is constant along any chord. The change in the fin's longitudinal center of pressure due to a change in the radial center of pressure will be determined by the slope of the ¼ chord line, so the longitudinal center of pressure interference factor is

$$K_{TBCP} = 1-\left(\left(1-k_{TBCAR}\right)\cdot\tan\left(\Gamma_Q\right)\right) \tag{3.11-8}$$

At a ¼ chord slope of 45 deg, the gain between a change in the radial center of pressure and the longitudinal center of pressure is 1. Figure 3-23 shows a plot of equation (3.11-8) vs $1/\tau$ for two values of λ at a ¼ chord line slope of 45 deg.

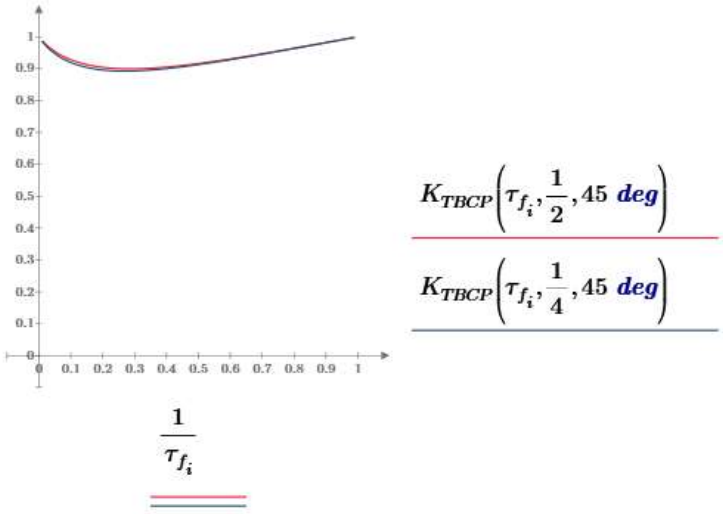

Figure 3-23 Longitudinal Center of pressure tail-body interference factor for $\Gamma_q = 45\,\text{deg}$ and $\lambda = 1/2$ and $\lambda = 1/4$

Figure 3-24 shows a plot of the longitudinal center of pressure interference factor for $\lambda = 1/4$ and 4 values of the ¼ chord line slope. If the slope of the ¼ chord line is less than 45 deg, then the center of pressure will change less than k_{TBCAR}, and if the slope is more than 45 deg, the longitudinal center of pressure will change more than k_{TBCAR}. For most fins, the ¼ chord slope is probably 45 deg or less, so, indeed, the tail-body interference can be neglected in most cases when calculating the fin center-of-pressure.

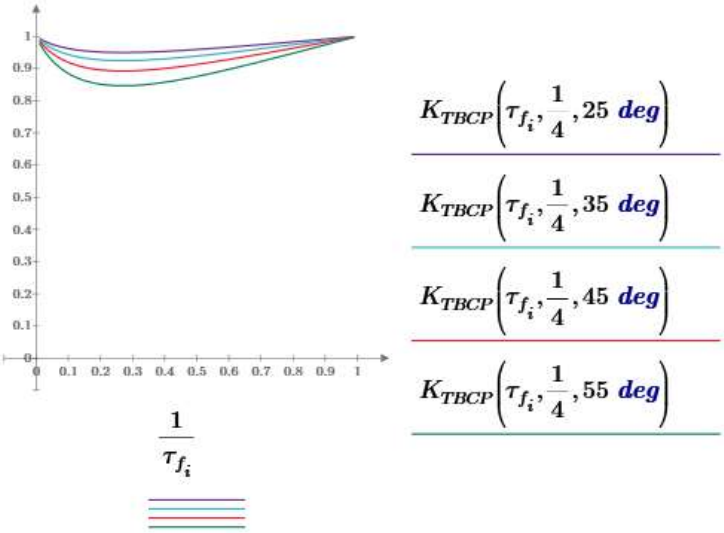

Figure 3-24 Longitudinal Center of pressure tail-body interference factor for $\lambda = 1/4$ and $\Gamma_Q = 25 - 55\,\text{deg}$

The moment due to just the fins is the distance from the fin's center of pressure to the center of gravity of the rocket. Since both the center of pressure and center of gravity of the rocket are measured from the tip of the nosecone, the center of pressure for the fins is the distance from the tip of the nosecone to the tip of the root edge of the fin plus the distance from the tip of the root edge of the fin to the fin's center of pressure. Adding both the tail-body interference factor and the fin offset to equation (3.11-4), the complete expression for the fin center of pressure is

$$L_{CPf} = K_{TBCP} \cdot \left(\frac{c_b}{3} \cdot \left(\frac{c_r + 2 \cdot c_t}{c_r + c_t} \right) + \frac{1}{6} \cdot \left(c_r + c_t - \frac{c_r \cdot c_t}{c_r + c_t} \right) \right) + L_f \tag{3.11-9}$$

4 Fins Plus Canards

4.1 Configuration of the Vertical Orientation Control Rocket

There are three common configurations used for rocket orientation control, forward mounted control canards with rear mounted fixed fins, fin tabs on the rear of fixed fins, and control canards mounted behind the fixed fins. The parameters presented in this paper will work for all three configurations. Rear mounted control fins could be used as the control surfaces where the entire fin is rotated, but the gain using the entire fin is usually too large to be practical.

There are tradeoffs for each configuration. All three configurations have been used for high power rockets, but it is generally more practical to use canards mounted toward the front of the rocket for control of model and high power rockets. This allows space for mounting the canards directly on the shafts of the servo motors, eliminating the need for complex linkages or drive shafts with gears that add backlash, and allows designing the control unit including canards, servo motors, and electronics as a single, self-contained unit that can be conveniently tested outside the rocket. Forward mounted canards with fixed rear fins is the configuration that is used for test rocket VTS-1 and will be examined in this section.

Figure 4-1 shows a typical configuration for a rocket with control canards and the canard rotations used for roll and pitch control. To simplify the control, four control canards are used along with three separate control systems, one for pitch, one for yaw, and one for roll. To control pitch, the two y-axis canards are moved as a pair in the same rotational direction on the y-axis. To control yaw, the two x-axis canards are moved as a pair in the same rotational direction on the x-axis. Because the yaw and pitch canards are orthogonal, the roll and pitch control systems are independent, simplifying their design. For roll control, all four canards rotate together with the opposite canards rotating in opposite directions on their respective axes. For calculating the pitch and yaw normal force, only two canards and fins are used for each, but for roll, all four fins and canards are used.

So far, all the aerodynamic parameters, forces, and moments have been determined for fins. Canards are simply smaller fins, so all the parameters that apply to the fins also apply to the canards, the only difference being their size and location along the body of the rocket.

Since the canards are ahead of the center of gravity in this configuration, the moment arm between the canard's center of pressure and the rockets center of gravity will have the opposite sign as the fin's moment arm. A positive rotation of the forward mounted y-axis canard will cause a positive y-axis pitch moment and rotation about the rocket's center of gravity, the opposite effect the fins would have. The forward canard location has no effect on roll control.

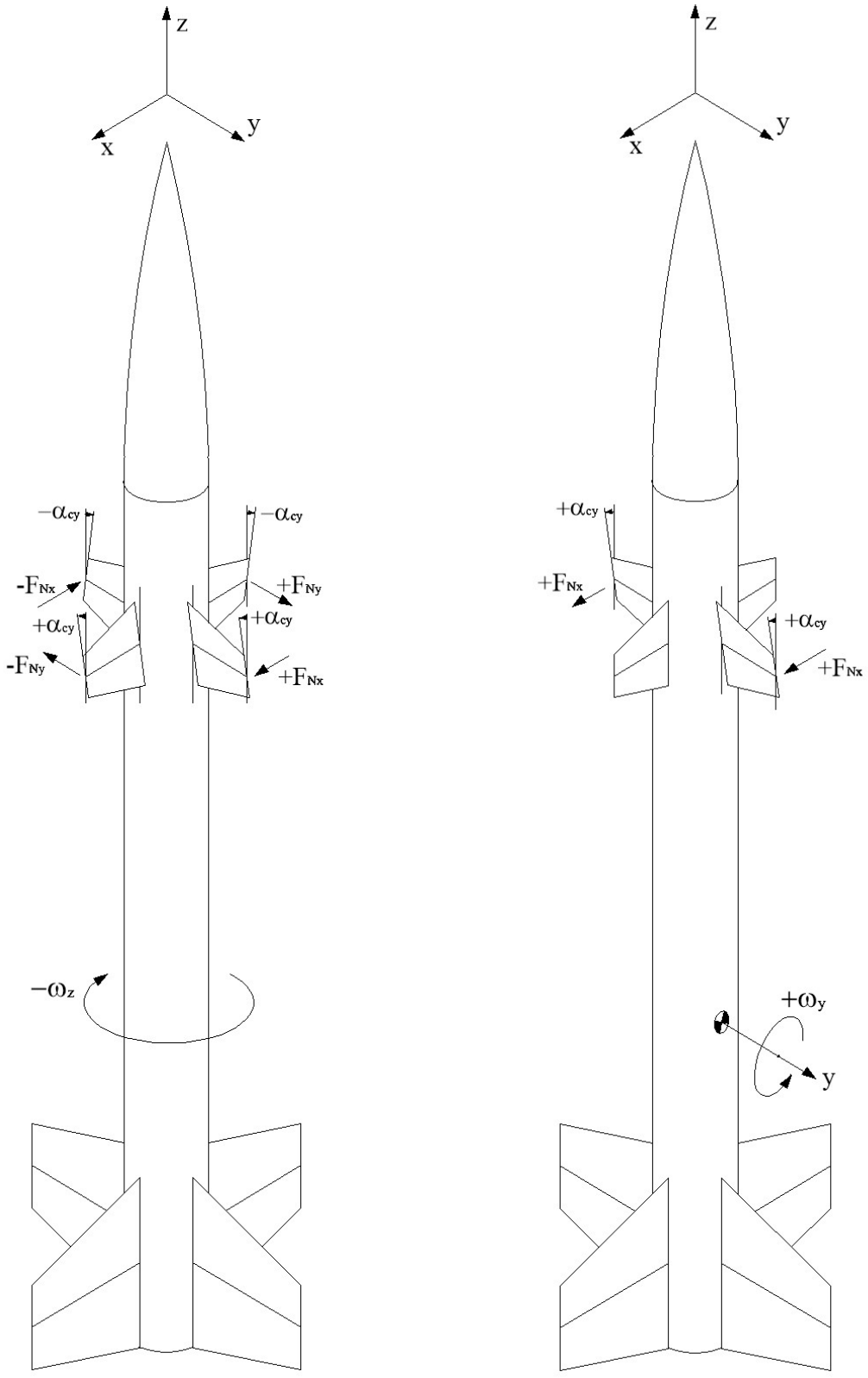

Figure 4-1 Typical vertical orientation control rocket configuration showing roll and pitch control

4.2 Impact of Canard Downwash on Roll Parameters

Figure 4-2 shows a simulation of the roll rate of a rocket when 2 canards are rotated 8 degrees for the vertical orientation test rocket VTS-1. The physical dimensions of VTS-1 are described in Appendix 2. A complete description of the model equations and the flight simulator will be given in a future paper, but the flight simulator uses the aerodynamic fin parameters described in this paper. For this test, VTS-1 was configured with just 2 opposing canards. The 2 canards are moved from 0 to 8 degrees rotation and then back to 0. There is no control loop involved, so it is called an open loop step response test which is used to measure the roll rate gain (radians/sec/degree of canard rotation) of the canards. The roll rate is a function of the velocity of the rocket, and this can be seen in the simulation data. When the canards are first rotated, the change in spin rate follows an exponential rise time, reaching a final step value of 3 rev/s, and then it slows down as the rocket velocity decreases after motor burnout at 1.5 s.

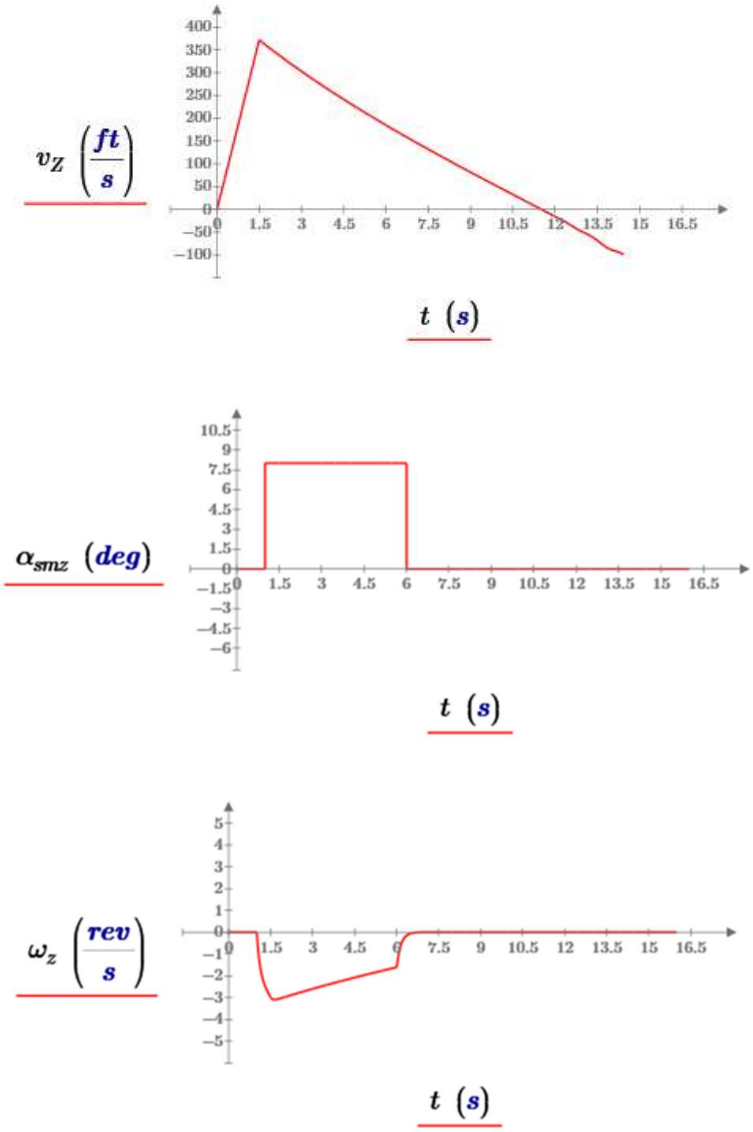

Figure 4-2 Simulation of spin rate response for VTS-1 showing the vertical velocity, the spin rate, and the angle of the canards

Figure 4-3 shows the results from a flight of VTS-1 where the two canards are rotated 8 degrees in opposite directions and back, compared to the simulated flight from above. The change in spin rate as the canards are stepped is only about 0.6 rev/s, about 1/5 the spin rate of the simulation. The rocket has already started to spin before the canards were stepped, probably due to airframe asymmetries or thrust imbalance, which is not unusual, so the change in rotation rate when the canards are stepped is the value used for the rotation rate step. It can also be

seen that the rotation rate does not change significantly as the rocket slows after motor burnout, which occurs at 1.5s.

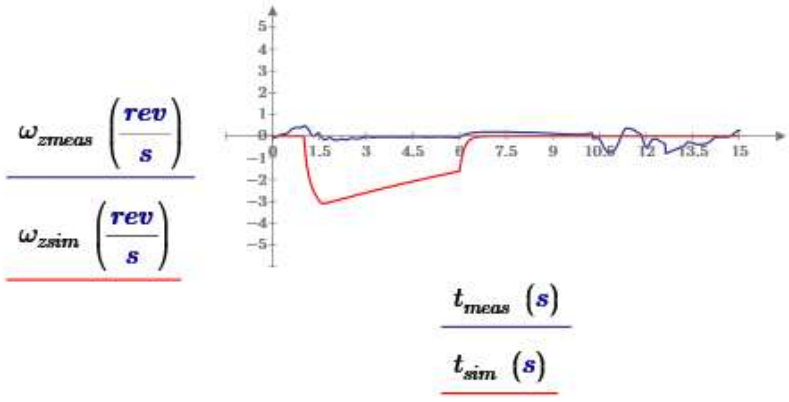

Figure 4-3 Spin rate simulation and flight data for VTS-1 Flight 7

The significantly lower effectiveness or gain of the canards is due to an interaction between the canards and the fins. Barrowman[45] does not cover this interaction, but Pitts, Nielsen, & Kaattari[46] does for the case of a forward wing and a rearward tail, which also applies to the canard/fin topology.

The simplest model that describes what is happening is shown in Figure 4-4. As the airstream passes over the rotated canards, the airstream is redirected by the angle of the canards. In this model, the downwash is flat and coplanar to the canards and fins, so it simply looks like an airflow at an angle-of-attack to the fins that is the same as the rotation angle of the canards within the span of the canards as shown in Figure 4-4. The redirected airflow is called a flat vortex sheet[47]. The normal force on the fins due to the downwash will be in the opposite direction of the normal force on the canards due to the canard's rotation angle.

[45] (Barrowman J. S., 1967)

[46] (Pitts, Neilsen, & Kaattari, 1957, pp. 576-581, 614, 619-624)

[47] (Nielsen, 1988, p. 182)

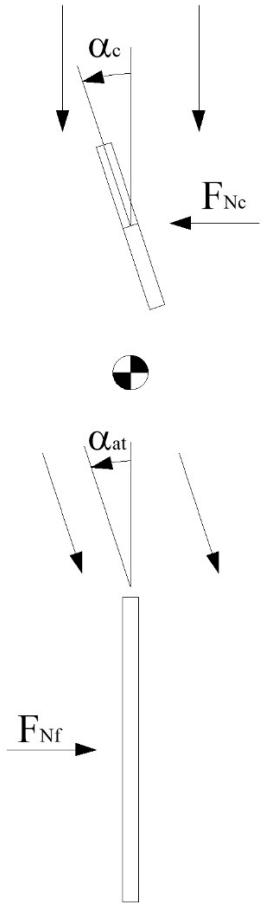

Figure 4-4 Downwash from the canards creates an angle-of-attack on the fins

Figure 4-5 shows the symmetry of the normal forces when the canards are angled for roll control and the impact to the roll moment. For roll, opposite canards are rotated in opposite directions. Because, for roll, the opposing normal force from the canards and the downwash normal force on the fins are on the same side of the radial centerline of the rocket, the net roll moment will be due to the difference between the canard and fin normal forces. If the downwash normal force on the fins is less than the normal force on the canards, then the roll moment is reduced so the effectiveness of the canards is reduced, but still in the direction expected for the angle of rotation of the canards. If the downwash normal force on the fins is greater than the normal force on the canards, the roll moment is reversed, and the rocket will roll in the direction opposite the intended direction, reversing the sign of the canard gain. If this happens when the canards are being used in a control loop to control the roll, the loop will go unstable.

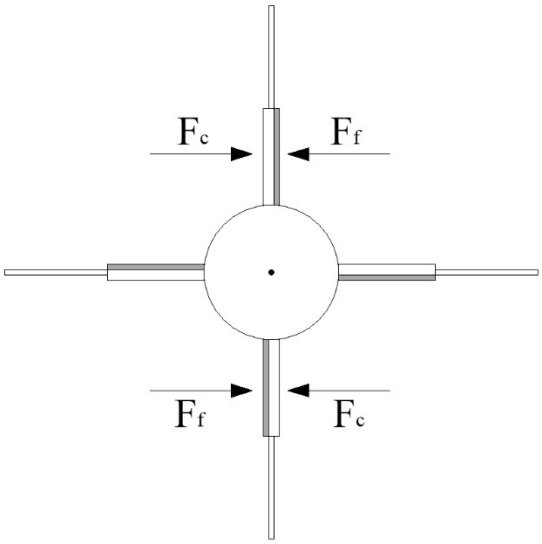

Figure 4-5 Symmetry of the normal forces created by roll control

Figure 4-6 shows the symmetry of the normal forces when the canards are angled for pitch control and the impact to the pitch moment. For pitch, opposite canards are rotated in the same direction. For pitch, the opposing normal force from the canards and the downwash normal force on the fins are on the opposite side of the longitudinal center of gravity of the rocket for the configuration shown in Figure 4-1 and Figure 4-4. The normal forces will add constructively and the pitch moment will be due to the sum of the canard and fin normal forces, so the interference increases the effectiveness of the canards.

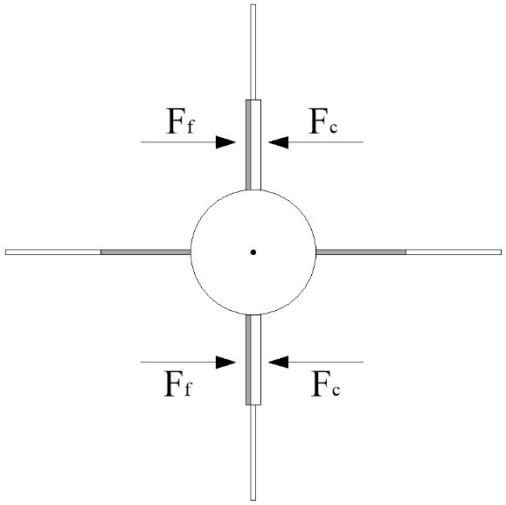

Figure 4-6 Symmetry of the normal forces created for pitch

If the canard-fin interference were simply due to a redirect airflow, it would be easy to calculate the lift on the fins over the span of the canard using the rotational angle of the canards as the angle-of-attack on the fins over the span of the canards as shown in Figure 4-7.

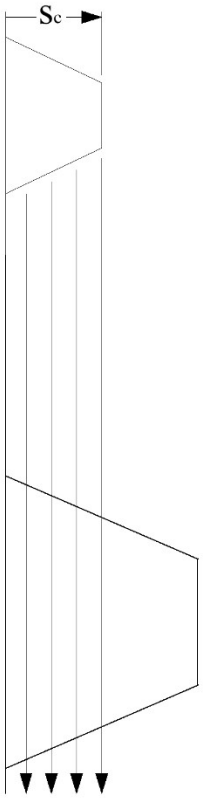

Figure 4-7 Span of sheet vortex downwash that affects fin

But, in most cases, rather than just changing the angle of the airstream over the span of the canard in a flat sheet, a more complicated spiral vortex is created at the tip of the canard, that trails behind the canard, as shown in Figure 4-8. Inside the tip of the canard, the air flows in the direction as deflected by the angle of the canard. Outboard, the air circles back in the opposite direction, forming the circular vortex. This has a similar effect as the sheet vortex, but the lift on the fin is much harder to calculate. Adding to the complexity, multiple vortices can be created by the canards that modify the lift of the fins depending on their size and location as they pass over the fins. The vortices can leave the canard at an angle to the longitudinal axis of the rocket, further complicating the calculation of their impact on the fins

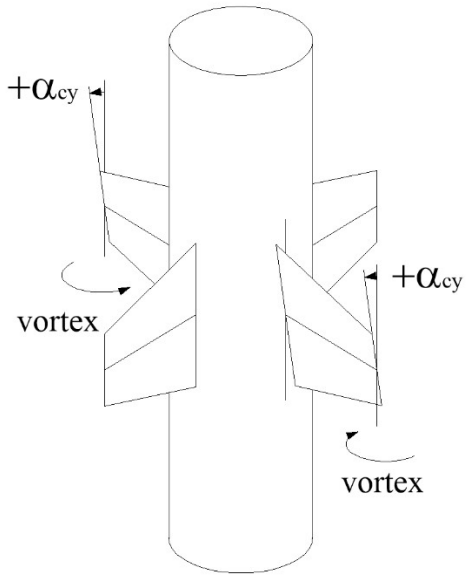

Figure 4-8 Tip vortices created by angled canards

Pitts et al quantifies the effect of the canard downwash due to tip vortices as a lift coefficient for the fins as[48]

$$C_{NTV} = \frac{C_{N\alpha 1c} \cdot C_{N\alpha 1f} \cdot \left(K_{TBc} \cdot \alpha_{at} + \alpha_c\right) \cdot i_f \cdot s_f}{2 \cdot \pi \cdot AR_f \cdot f_c} \tag{4.2-1}$$

(for this paper, Pitts' wing parameters are replaced by the canard parameters, and the tail parameters are replaced by the fin parameters). Pitts et al uses the lift coefficient, but it is assumed that the normal force coefficient equals the lift coefficient. Dividing equation (4.2-1) by the angle-of-attack gives the downwash normal force coefficient derivative as

$$C_{N\alpha TV} = \frac{C_{N\alpha 1c} \cdot C_{N\alpha 1f} \cdot i_f \cdot s_f}{2 \cdot \pi \cdot AR_f \cdot f_c} \tag{4.2-2}$$

[48] (Pitts, Neilsen, & Kaattari, 1957, p. 581 eq (45))

In this equation, there are two parameters that describe the location of the vortex on the canard and fin. f_c describes the radial location of the center of the vortex on the canard, and i_f describes the fin interference factor which is dependent on the height of the vortex over the fin[49].

All of the values in equation (4.2-2) come from the rocket dimensions or can be calculated from equations already presented, except for f_c and i_f. Calculating those two values is complicated, but Pitts et al provides graphs of estimates for those values that can be used to evaluate equation (4.2-2) based on a range of forward canard (wing) and rearward fin (tail) geometries.

Charts 5 and 6 in Pitts et al[50] show the radial location of the vortex on the forward canard vs the effective aspect ratio for different values of tip chord to root chord or λ. The vortex location f_w, or f_c in this paper, is given as the radial position normalized to the wing or canard span, such that

$$X = \frac{f_w - r_w}{s_w - r_w} = \frac{f_c}{s_c} \tag{4.2-3}$$

Chart 7[51] gives the value of the fin interference factor, i_f, as contour lines on a graph of the vertical position of the vortex on the fin, versus the lateral position of the vortex on the fin. For VTS-1, the tip to root chord ratio is $\lambda_c = 0.5$. Pitts et al Chart 5 shows the normalized location of the vortex on the canard is $X \simeq 0.8$ for any value of effective aspect ratio when $\lambda = 0.5$. So, from equation (4.2-3), for $s_c = 2in$, $f_c = 1.6in$. For VTS-1, $\lambda_f = 0.5$ and $1/\tau_f = 0.281$, so choosing Chart 7(f) as the closest, then a contour line of $i = -1.0$ appears to be in the middle of the range when the lateral and vertical normalized vortex positions are around 0.8-1.0.

With these values, the normal force coefficient derivative from equation (4.2-2) for a fin due to the downwash from a canard is $C_{N\alpha TV} = -1.222$. For VTS-1, the normal force coefficient derivative for a canard is $C_{N\alpha 1c} = 1.23$, so, according to this analysis, the normal force on the fins due to the downwash is the same magnitude but opposite the normal force created by a canard per equation (4.2-1) for any small rotation angle of the canard, for a net normal force and rotational moment of zero. If i were smaller in magnitude, the canards would have reduced effectiveness,

---

[49] Note that Pitts et al references s_w, f_w, and s_T from the radial center line, or z-axis, and then subtracts the radius of the body at the wing, r_w, or tail, r_T from all three in the calculations. This paper references s_c, f_c, and s_f from the radius of the body tube, so there is no need to subtract r_t, the radius of the body tube.

[50] (Pitts, Neilsen, & Kaattari, 1957, pp. 617-618)

[51] (Pitts, Neilsen, & Kaattari, 1957, pp. 619-624)

and if i were larger in magnitude, the canards would have a reverse effect, the rocket would roll in the direction opposite the expected direction for a given rotation angle on the canards.

Note that the Pitts analysis calculates the downwash normal force coefficient for the fin. The location of the vortex over the fin sets the moment arm for calculating the resulting roll moment. Calculating the effective moment arm is not included in Pitts analysis above.

Looking at the flight data from Figure 4-3, it can be seen that the spin rate does not change with the velocity of the rocket, rather it is fixed for most of time the canards are angled, so it appears the canards have little effect on roll, which generally agrees with the results using equation (4.2-1). It is impossible to determine exactly how effective the canards are from the flight data because the external forces driving the roll rate of the rocket are not known But what appears to be happening is that the gain of the canards changes over the 6 seconds they are set to 8 degrees, probably because the location of the vortices changes as a function of the velocity of the rocket, which would change the values of f_c and i .

Even though the Pitts et all model of the downwash vortices does not result in a complete or precise value for the effect of the downwash, the analysis does show that there is some physical justification that the phenomenon of circular vortices shed from the canards can be the cause of the results obtained from the flight data.

4.3 Impact of Canard Downwash on Pitch Parameters

For pitch, as shown in Figure 4-4 , the symmetry of the normal force due to the canard downwash is such that the effectiveness of the forward canards should be increased.

It is not practical to do an open loop step response of the canards to measure the pitch or yaw rotation rate because that would put the rocket into an unsafe circular flight path. Instead, the closed loop pitch and yaw response to the step in the oncoming wind velocity as the rocket leaves the launch guide is used.

Figure 4-9 shows the measured flight data, along with the 3D flight simulation, for flight 14 of VTS-1, which used both pitch and roll control. The simulation uses the same control loop parameters as the VTS-1 flight controller. The downwash effect was not included in this simulation. The initial peak due to the wind as the rocket left then launch guide occurs a little faster than the simulation, but the overall match is very close. The size of the initial rotation and the time to correct back to zero is a very close match.

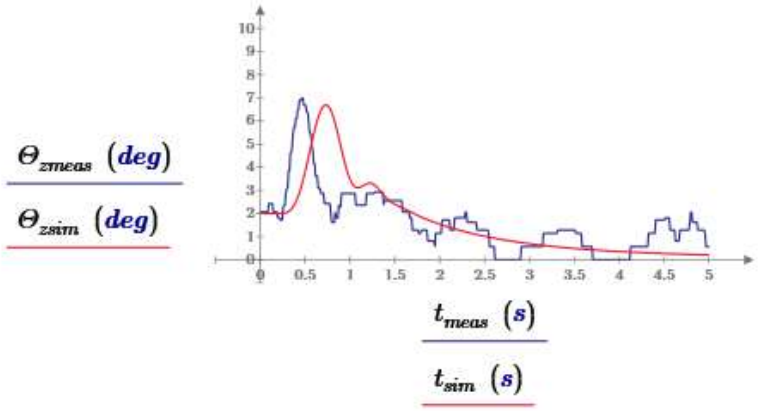

Figure 4-9 $K_{TV} = 0$, no downwash

Figure 4-10 shows the same flight data but compared to a simulation that includes the effects of the canard downwash using the same value for $C_{N\alpha TV}$ as calculated above. The effectiveness of the canards for pitch control is effectively doubled since the distance from the canard center of pressure to the rocket's center of gravity is very close to the distance from the fin's center of pressure, the location of the canard's negative image, to the rocket's center of gravity. Doubling the gain of the canards without changing the control loop parameters increases the bandwidth of the control loop so that the loop responds faster to the cross wind perturbation, reducing the pitch/yaw error.

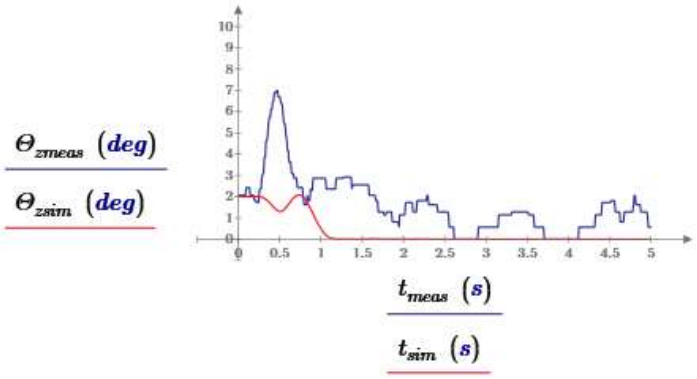

Figure 4-10 $K_{TV} = -1$

The simulation without the downwash effect is a much closer match to the flight data than the simulation with the downwash. Indeed, any increase in the effective gain of the canard would negatively impact the accuracy of the

simulation. This says that the downwash has very little effect on the effectiveness of gain of the canards for pitch control.

The canard downwash could also impact the rocket's stability by affecting its longitudinal center of pressure. Equation (4.2-1) shows that the canard downwash creates a normal force on the fins both due to the rotational angle of the canards as well as the angle-of-attack of the rocket. Figure 4-11 shows the fin and canard related normal forces. The normal force due to the canard downwash on the fins would move the rocket center of pressure forward because it has the opposite sign of the normal force due to the fins. This would negatively affect the rocket's longitudinal stability. But the pitch rotation flight data shows that the rocket's stability matches the flight stability prediction using the fins and canards without including any effects of the downwash.

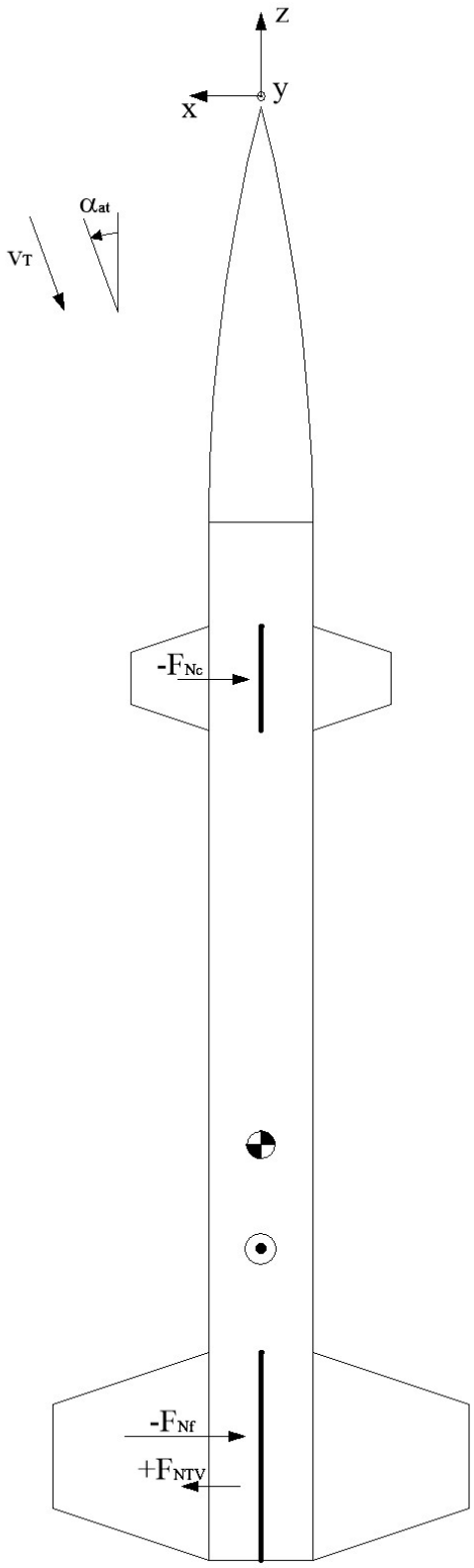

Figure 4-11 Canard downwash impact on fin normal force due to rocket angle-of-attack

4.4 Rocket Configurations for Roll Control

The canard downwash makes the canards unusable for roll control because, at best, the effective gain is indeterminate, and at worst, the sign of the gain can reverse, either case making it impossible to design a control loop with deterministic behavior. The solution to the roll control problem for VTS-1 is to use a freely rotating fin can, or "spin-can", a term coined in Jim Jarvis' vNARCON 2023 presentation [52]. The earliest found reference to free-rolling tail fins is a 1978 NASA technical report by Blair[53] for a wind tunnel test model. Blair cites an earlier reference to the use of a freely spinning tail from 1972 by Darling, but that article could not be found. Although Blair's design is for a wind tunnel model, it is surprisingly close to the designs being used for high power rockets by Jim Jarvis and the author. More details about the design of the VTS-1 spin-can will be presented in a future paper.

The spin-can eliminates the downwash interference from the canards because the fins cannot generate a counter torque on the rocket if they are free to spin. There is no impact on the effectiveness of the fin pitch forcing and damping moments because the pitch normal forces are equal on either side to the z-axis center line of the rocket as shown in Figure 4-6.

A second possible solution for roll control tested by Blair et al[54] using a wind tunnel model has fins that have a span that is significantly less than the span of the canards. With a fin span less than the forward canard span, the hypothesis is that only a portion of the canard downwash falls within the span of the fins, so only a portion of the canard normal force is counteracted by the downwash normal force on the fins. This method has not been tried by the author, but the wind tunnel results for this configuration from Blair et al are examined in the next section.

4.5 NASA Wind Tunnel Test Data

Blair presents the test results from a wind tunnel model for the effects of forward canards and fixed and free-rolling fin/tail sections on the longitudinal and radial aerodynamic characteristics of the rocket in his 1978 NASA technical paper[55]. The configuration of the wind tunnel model is similar to the configuration of VTS-1, where the span of the canards is about half the span of the fins. Blair's test results can be used to further validate whether the canard downwash impacts the roll and pitch dynamics of a rocket. Blair's paper draws three conclusions; that the fixed

---

[52] (Jarvis, 2023)

[53] (Blair A. B., Wind_Tunnel Investigation at Supersonid Speeds of a Canard-Controlled Missile With Fixed and Free-Rolling Tail Fins, 1978)

[54] (Blair, Dillon, & Watson, September-October 1993)

[55] (Blair A. B., 1978)

and free rolling configuration have about the same longitudinal lift force coefficient and stability, that the free rolling tail configuration allows roll control using forward canards, and the free rolling tail configuration reduced the induced roll due to canard yaw control. The first two conclusions agree with the flight results seen with VTS-1. The third conclusion would be hard to verify from flight data where roll, pitch, and yaw are all being controlled.

The test case in Blair for using the canards with and without the free rolling tail for roll control only uses a small 0.5 deg rotation of the canards[56], which produces a very small change in the roll moment coefficient for the free rolling fins case. But for the fixed tail, the 0.5 deg canard rotation produces a larger moment in the opposite direction, which would cause control reversal. This confirms that the canards are not effective for roll control when using a fixed fin section.

Blair measures the longitudinal lift on the test model with the canards but does not compare that measurement to a model's prediction with and without the effects of the canard downwash, so does not determine whether the downwash impacts the lift. Figure 9-1 in Appendix 3 of this paper shows the calculation of the normal force for Blair's wind tunnel test model using the fin parameters presented in this paper, including the body/tail interference factor, but without the downwash interference factor. The calculations show that, at an angle-of-attack of 4 deg, the lift/normal force coefficient derivative is 1.6. This is calculated at Mach 1.7, the lowest of the wind tunnel test velocities in Blair, using Barrowman's adjustment to the fin lift equation that accounts for the velocity greater than Mach 1. Looking at Blair[57], for two different roll orientations of the rocket, the measured value of the lift coefficient at 4 deg is around 1.6-1.7, which agrees with the calculation in Appendix 3 that does not include any effects of downwash. Blair's results for the longitudinal lift are the same with and without the free rolling fin section.

Both the flight data from VTS-1 and the wind tunnel measurements from Blair, therefore, show that the downwash from the canards significantly impacts the effectiveness of the canards for roll control, but has almost no impact on the effectiveness of the canards for pitch control.

Blair et al suggests that flow field produced by differential deflected canards, used for roll control, engulfs the tail fin region[58]. A difference in the flow patterns between differential and common mode deflection of the canards could be the cause of the difference between the interference impact on the fins for pitch and roll, but no attempt was made by Blair to measure the relative flow patterns in the wind tunnel tests.

---

[56] (Blair A. B., 1978, p. 65 figure 11a)

[57] (Blair A. B., 1978, pp. 26, Figure 4, p 34, Figure 5)

[58] (Blair, Dillon, & Watson, September-October 1993, p. 638)

Based on VTS-1 flight data and the NASA wind tunnel model test data, it appears that, for a rocket that uses forward mounted canard and a free rolling fin section, or spin-can, there is no need to include a canard/fin downwash interference factor in the aerodynamic parameters for either the roll or the pitch parameters.

Another method of minimizing the impact of canard downwash is to increase the span of the canards relative to the span of the fins. In their 1993 paper[59], Blair et al present the test results for a wind tunnel model with a fin span significantly less than the forward canard span. That paper shows that as the fin span is reduced to less than the canard span, the effective net rotational normal force coefficient for the rocket increases significantly. At a fin span to canard span ratio of 0.47, the magnitude of the rotational normal force coefficient is about 1.2 for a canard rotation angle of 5 deg[60]. The rotational force coefficient assuming no effects of the canard downwash is calculated in Figure 9-2 of Appendix 3 of this paper to be 1.98, so the measured value is about 60% of the calculated value without downwash. This reinforces the idea that the downwash directly trails the canard a shown in Figure 4-7. This could make the canards effective enough to be used for roll control, but the wind tunnel test results show that the normal force does change with velocity at larger angles-of-attack. All these measurements were made above Mach 1, so additional testing would be needed to validate the consistency of the normal force for subsonic velocities.

The practical limitation of this method is the resulting location of the center of pressure for the rocket. The center of pressure for the wind tunnel test model with the fin to canard span ratio of 0.47 is at a distance that is 34% of the total rocket length from the tip of the nosecone, which would be well ahead of the center of gravity for any practical rocket. Keeping the area of a fin constant, the normal force coefficient increases roughly linearly with the aspect ratio. Setting the span of the canards wider than the span of the fins increases the lift of the canards relative to the fins and moves the center of pressure forward significantly, making this an impractical solution to the canard effectiveness problem.

---

[59] (Blair, Dillon, & Watson, September-October 1993, pp. 639, Fig 8a)

[60] In an earlier paper (Blair, Allen, & Hernandez, June 1983, p. 31 Figure 8a), the same figure was published, but stating the canard rotation angle was 10 deg which would halve the effective roll moment coefficient

5 Simulation vs. Flight Data Results

The control fin aerodynamic parameters presented in this paper were used to design the control system for a vertical orientation rocket. The accuracy of the aerodynamic parameters is determined by comparing the flight date from the rocket to the 3-D simulation of rocket's flight as shown in Figure 5-1. The flight simulator is a time domain simulator that includes the aerodynamic rocket model, a dynamic model of the servo motors, and the same control loop functions for pitch, yaw, and roll control that are used in the actual rocket control system. If the aerodynamic parameters do not match the actual forces on the rocket, then the flight simulation will not match the flight data.

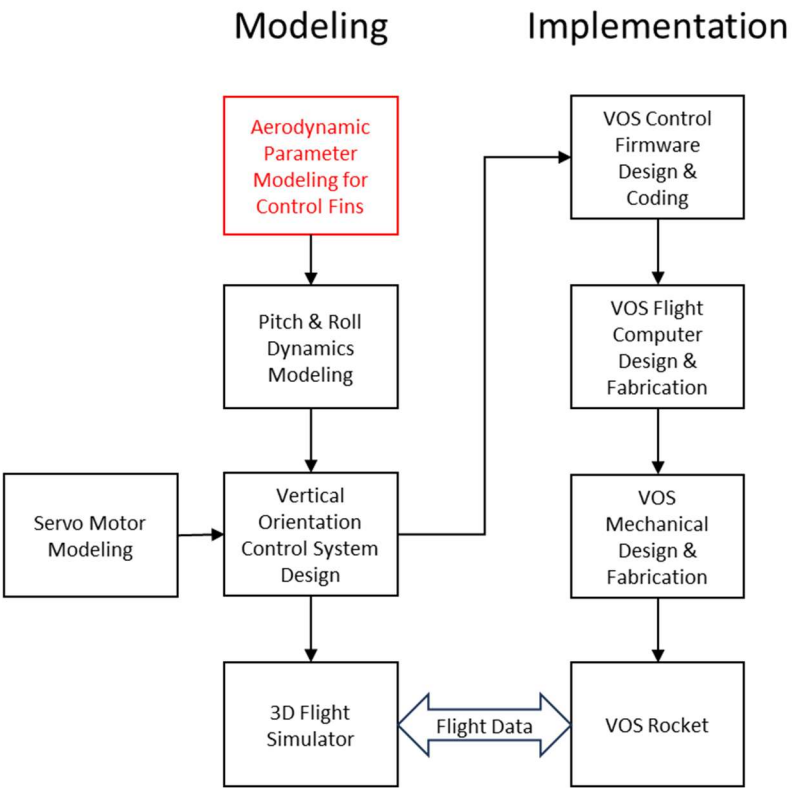

Figure 5-1 Design Process and Model Validation

Figure 5-2 to Figure 5-4 show the simulated and measured flight data for flight 14 of VTS-1 that took place on May 15, 2025, at LDRS, sponsored by TCC in Helm, California. Figure 5-2 shows the roll response. The roll control is a variable gain, optimal state space controller where the poles are held at a fixed optimal location independent of the rocket's velocity by changing the gain as a function of the rocket's velocity. More about the control system design and performance will be covered in the paper on the vertical orientation control system design.

The rocket started out 65 degrees from its absolute target roll angle which was having the positive rocket x-axis pointed due west. The fall time of the simulated response is a little faster than the flight data, and the damping is a little larger, but this is a very close match. In both cases, once the roll reaches the target 0 deg, the controller holds the absolute roll angle at zero without any oscillation due to loop instability. The well controlled response and close match between the simulation and flight data is achievable only if the aerodynamic parameters and rocket rotational dynamics are modeled correctly.

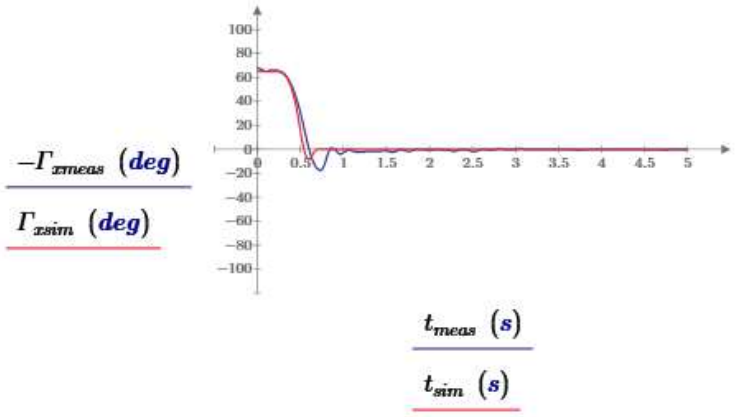

Figure 5-2 Simulated and measured flight data roll response for an initial offset of 65 deg

Figure 5-3 shows the same flight as Figure 5-2, but with the servo motor simulation enabled in the flight simulator. The servo motor model includes the servo motor dynamics as well as nonlinear attributes such as quantization and dc motor hysteresis. The step response shows a larger magnitude oscillation than the simulation without the servo motor. The oscillation caused by the servo motor is due to a limit cycle oscillation rather than the control loop stability dynamics. A limit cycle oscillation is caused by nonlinearities in a control loop. The servo motor model slightly overestimates the effects of the limit cycle oscillation, but it shows that some of the underestimation of the oscillation magnitude in Figure 5-2 is likely due to the servo motor and not a discrepancy in the calculation of the rocket's aerodynamic parameters.

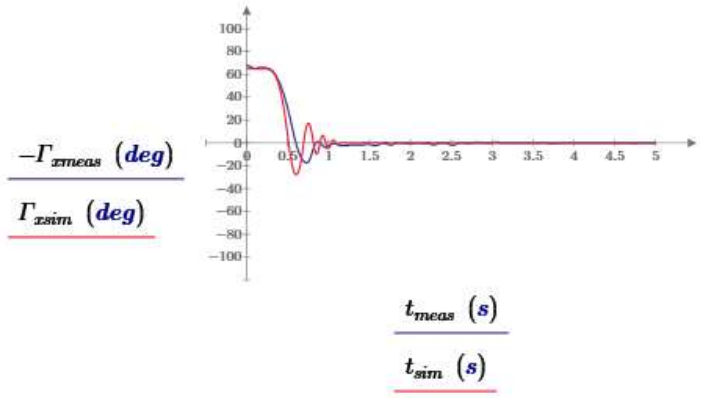

Figure 5-3 Simulated and measured flight data roll response for an initial offset of 65 deg with the servo motor dynamics simulation enabled

Figure 5-4 shows the tilt response. The pitch and yaw control is a fixed gain state space controller where the poles move as a function of the rocket's velocity but are optimized in the center of the rocket's velocity range. Tilt is the polar angle of the rocket's z-axis from vertical and includes the effects of both pitch and yaw rotations. The initial tilt of the launch rail is 2 deg, and the average ground wind speed at launch was ~15 mph. The initial conditions for the wind velocity in the simulation to get a good match with the flight data for the peak rotation is 20 mph. The measured initial rotation of the rocket as the rocket leaves the launch guide occurs earlier than the simulation, but the settling time back to zero is almost identical. The earlier rotation could be due to rail whip which would explain why a larger wind velocity was needed for the simulation to match the flight data. The flight data has about 1 deg of noise, most likely due to changes in the wind velocity which is not in the simulation. Overall, this is a very close match. Again, there is no instability in the control loop.

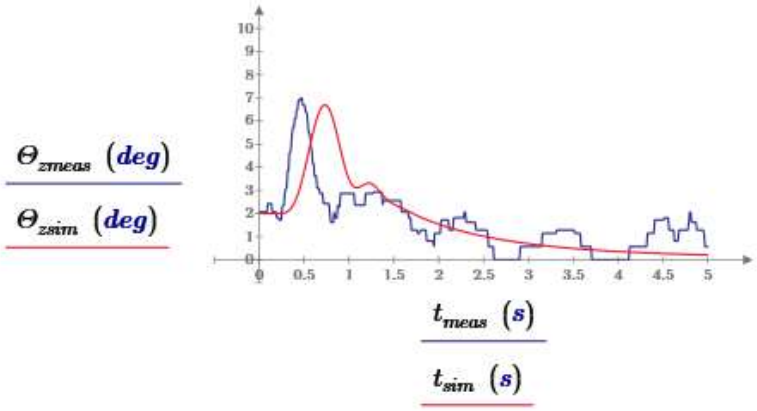

Figure 5-4 Simulated and measured flight data tilt response for an initial launch angle of 2 deg

6 Conclusions, and Next Steps

6.1 Conclusions

All the aerodynamic fin parameters needed to design and model a vertical orientation control system and a rocket flight simulator have been presented. The fin parameters and tail-body interference factors are summarized in Appendix 1.

It was shown that the flight data from the vertical orientation test rocket VTS-1 matches the 3-D flight simulator data very closely for steps in both tilt (pitch & yaw) and roll. The vertical orientation control system was designed using the aerodynamic parameters for the canards presented in this paper. The control system is implemented in both the 3-D flight model and the VTS-1 flight controller. The well controlled response and close match between the simulation and flight data is achievable only if the aerodynamic parameters and rocket rotational dynamics are modeled correctly.

It was also shown from VTS-1 flight data and NASA wind tunnel model test data that there is significant interference due to canard downwash on the fixed fins for roll control, but almost no interference for pitch control. This shows that a spin-can is required for effective roll control if the control canards are ahead of the fins, and that the aerodynamic parameters without a canard/fin interference factor can be used to accurately model the pitch control.

6.2 Next Steps

- Write the remaining papers to complete the documentation of the vertical orientation control project
- Calculate the pitch damping force and moment using the actual tangential velocity and induced angle-of-attack along the length of the chord of the fin rather than assuming a fixed value based on the angle-of-attack at the center of pressure of the fin to verify that using the fixed angle-of-attack at the fin's center of pressure location is a valid assumption

6.3 Summary of Key New Results Presented in This Paper

- Section 3.1: Derived the effect of dihedral angle on pitch normal force. Although Barrowman cites a NASA memo as the source of the equation, that memo is not available on the NASA Technical Report Server. It is shown that the total pitch normal force is independent of the roll angle of the rocket for any number of fins 3 or greater.
- Section 3.8: Showed that there is no roll damping tail-body interference
- Section 3.9: Determined the impact of the tail body interference on the calculation of the center of pressure and derived the center of pressure interference factor K_{TBCP}. Showed the impact is small and can be neglected in most cases.
- Section 3.6: Showed the total angle-of-attack for a control fin including the fin rotation angle and appropriate interference factors needed to calculate the pitch and yaw normal forcing and damping moments
- Section 3.9: Showed the total angle-of-attack for a control fin including the fin rotation angle and appropriate interference factors needed to calculate the roll normal forcing and damping moments
- Section 3.10: Showed that the radial center of pressure is the center of area of then fin which is an easier way to calculate the parameter
- Section 3.10: Introduced the radius of gyration parameter, CM_R, which is the equivalent moment arm for calculating the roll damping moment
- Section 3.10: Showed that the reference length in Barrowman's equation for the roll damping moment is the square root of the area of the fin. Knowing this is necessary to calculate the roll damping moment
- Section 4.2: Flight data showed that the canard downwash has a significant impact on the effectiveness of the canards to control roll but that it has little impact on pitch forcing moment
- Section 4.2: Applied the aerodynamic parameters from this paper to the Blair wind tunnel model to verify that the canard downwash has little impact on the pitch forcing moment in their test data
- All sections: The correct signs are given for the forces, moments, and rotational angles for yaw, pitch, and roll in the defined axis system

7 Appendix 1 - Fin/Canard Aerodynamic Parameter Summary

Parameter	Value	Source Equation
Normal Force on a single fin[61]	$C_{N\alpha 1f} = \frac{2 \cdot \pi \cdot AR \cdot \left(\frac{A_f}{A_r} \right)}{2 + \sqrt{4 + \left(\frac{AR}{\cos(\Gamma_c)} \right)}}$	(3.1-3)
Pitch Normal Force for N fins	$C_{N\alpha Tf} = \frac{N}{2} \cdot C_{N\alpha 1f}$	(3.1-9)
Roll Normal Force for N fins	$C_{N\alpha Rf} = N \cdot C_{N\alpha 1f}$	(3.1-12)
Center of Pressure Tail-body Interference Factor	$K_{TBCPf} \simeq 1$	(3.11-7) & (3.11-8)
Fin Center of Pressure	$L_{CPf} = K_{TBCPf} \cdot \left(\frac{c_b}{3} \cdot \left(\frac{c_r + 2 \cdot c_t}{c_r + c_t} \right) + \frac{1}{6} \cdot \left(c_r + c_t - \frac{c_r \cdot c_t}{c_r + c_t} \right) \right) + L_f$	(3.11-9)
Pitch/Yaw Tail-body Interference Factor due to body angle-of-attack	$K_{TBf} = 1 + \frac{1}{\tau} = 1 + \frac{r_t}{s + r_t}$	(3.2-9)
Pitch/Yaw Tail-body Interference Factor due to angle of fin	$k_{TBf} \simeq 1$	(3.3-1)[62]
Total Pitch Angle-of-Attack	$\alpha_{atey} = K_{TBf} \cdot \alpha_{aty} - k_{TBf} \cdot \alpha_{fy} - \frac{\omega_y \cdot \left(L_{CPf} - L_{CG} \right)}{V_T}$	(3.5-1)
Total Yaw Angle-of-Attack	$\alpha_{atex} = K_{TBf} \cdot \alpha_{atx} - k_{TBf} \cdot \alpha_{fx} - \frac{\omega_x \cdot \left(L_{CPf} - L_{CG} \right)}{V_T}$	(3.5-2)

[61] If the control surfaces are canards with fixed fins, the *f* subscript would be replaced with a *c* subscript for the canards to distinguish between the two

[62] If the interference factor is close to 1 and can me ignored in most cases, it is shown as 1 in this table. Refer to the source equations for the exact values for the approximated interference factors

Parameter	Value	Source Equation
Pitch Forcing Normal Force	$F_{N1xf} = -\frac{\rho}{2} \cdot A_r \cdot {v_T}^2 \cdot C_{N\alpha T} \cdot \left(K_{TB} \cdot \alpha_{aty} - k_{TB} \cdot \alpha_{fy} \right)$	(3.6-3)[63]
Yaw Forcing Normal Force	$F_{N1yf} = \frac{\rho}{2} \cdot A_r \cdot {v_T}^2 \cdot C_{N\alpha T} \cdot \left(K_{TB} \cdot \alpha_{atx} - k_{TB} \cdot \alpha_{fx} \right)$	(3.6-5)
Pitch Damping Normal Force	$F_{N2xf} = \frac{\rho}{2} \cdot A_r \cdot \lvert v_T \rvert \cdot C_{N\alpha T} \cdot \omega_y \cdot \left(L_{CPf} - L_{CG} \right)$	(3.6-4)
Yaw Damping Normal Force	$F_{N2yf} = -\frac{\rho}{2} \cdot A_r \cdot \lvert v_T \rvert \cdot C_{N\alpha T} \cdot \omega_x \cdot \left(L_{CPf} - L_{CG} \right)$	(3.6-6)
Pitch Forcing Moment	$M_{1yf} = \frac{\rho}{2} \cdot A_r \cdot {v_T}^2 \cdot \left(L_{CPf} - L_{CG} \right) \cdot C_{N\alpha T} \cdot \left(K_{TB} \cdot \alpha_{aty} - k_{TB} \cdot \alpha_{fy} \right)$	(3.6-9)
Pitch Damping Moment	$M_{2yf} = -\frac{\rho}{2} \cdot A_r \cdot \lvert v_T \rvert \cdot \left(L_{CPf} - L_{CG} \right)^2 \cdot C_{N\alpha Tf} \cdot \omega_y$	(3.6-10)
Yaw Forcing Moment	$M_{1xf} = \frac{\rho}{2} \cdot A_r \cdot {v_T}^2 \cdot \left(L_{CPf} - L_{CG} \right) \cdot C_{N\alpha T} \cdot \left(K_{TB} \cdot \alpha_{atx} - k_{TB} \cdot \alpha_{fx} \right)$	(3.6-11)
Yaw Damping Moment	$M_{2xf} = -\frac{\rho}{2} \cdot A_r \cdot \lvert v_T \rvert \cdot \left(L_{CPf} - L_{CG} \right)^2 \cdot C_{N\alpha T} \cdot \omega_x$	(3.6-12)
Total Roll Angle-of-Attack	$\alpha_{ats} = -k_{TBf} \cdot \alpha_f - \frac{\omega_z \cdot r}{v_{Tz}}$	(3.9-1)
Radial Center of Area	$CA_{Rf} = \frac{s}{3} \cdot \frac{2 \cdot c_t + c_r}{c_t + c_r} + r_t$	(3.10-12)
Radius of Gyration	$CM_{Rf} = \sqrt{\frac{\left(3 \cdot c_t + c_r\right) \cdot s^2 + \left(8 \cdot c_t + 4 \cdot c_r\right) \cdot r_t \cdot s + \left(6 \cdot c_t + 6 \cdot c_r\right) \cdot {r_t}^2}{6 \cdot \left(c_t + c_r\right)}}$	(3.10-16)
Roll Forcing Moment	$M_{1zf} = -\frac{\rho}{2} \cdot A_r \cdot {v_{Tz}}^2 \cdot CA_{Rf} \cdot C_{N\alpha Rf} \cdot k_{TBf} \cdot \alpha_f$	(3.10-9)
Roll Damping Moment	$M_{2zf} = -\frac{\rho}{2} \cdot A_r \cdot \lvert v_{Tz} \rvert \cdot {CM_{Rf}}^2 \cdot C_{N\alpha Rf} \cdot \omega_z$	(3.10-15)

[63] All the interference factors, including those that can be approximated by 1, are included to show which coefficients they apply to

8 Appendix 2 - VTS-1 Test Rocket

VTS-1 is the vertical orientation control rocket, including the custom flight controller, used to gather all the flight data presented in this paper. More information about the VTS-1 project is available on the author's web site[64].

VTS-1 rev4.1
Length: 59.4500 In. , Diameter: 3.1000 In. , Span diameter: 11.1000 In.
Mass 9.116673 Lb. , Selected stage mass 9.116673 Lb.
CG: 35.8127 In., CP: 40.3972 In., Margin: 1.48
Engines: [J350W-0]

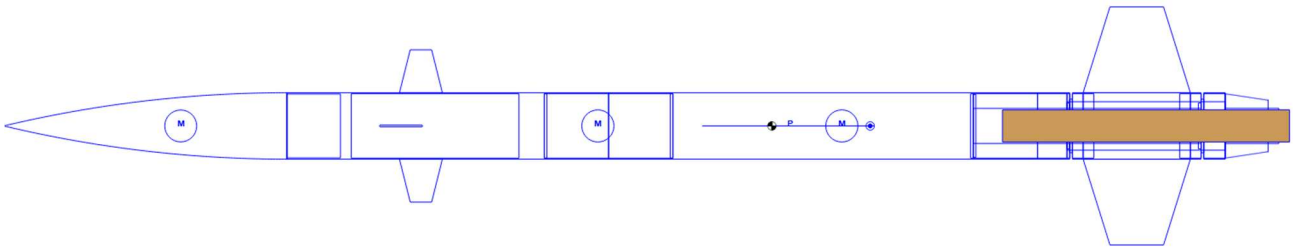

Rocket Diameter	$D_r = 3.124\ in$
Nosecone Length	$L_{nc} = 13.2\ in$
Body tube length	$L_{bt} = 46.25\ in$
Number of fins	$N_f = 4$
Fin root edge length	$c_{rf} = 5\ in$
Fin tip edge length	$c_{tf} = 2.5\ in$
Fin span from body tube	$s_f = 4\ in$
Fin mid cord sweep angle	$\Gamma_{cf} = 0\ deg$
Fin base location	$L_f = 3\ in$
Number of canards	$N_c = 4$
Canard setback length	$L_{sc} = 5\ in$
Canard root edge length	$c_{rc} = 2\ in$
Canard root edge length	$c_{tc} = 1\ in$
Canard span from body tube	$s_c = 2\ in$
Canard mid cord sweep angle	$\Gamma_{cc} = 0$
Mass of the rocket plus motor	$m_o(0 \cdot sec) = 8.955\ lb$
Longitudinal moment of inertia	$I_L = 14.369\ lb \cdot ft^2$
Lateral moment of inertia	$I_R = 0.087\ lb \cdot ft^2$
Center of gravity	$L_{CG_0} = 35.614\ in$
Center of pressure	$L_{CP} = 41.795\ in$

[64] (Fetter, 2025)

9 Appendix 3 –NASA Wind Tunnel Test Model Calculations

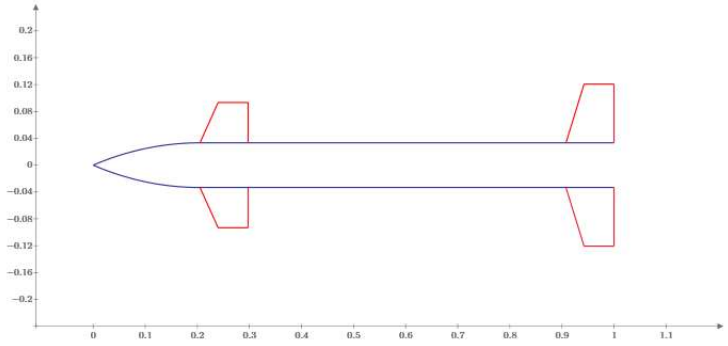

$D_r = 2.6\ in$

$c_{rc} = 3.6\ in$ $\quad c_{rf} = 3.6\ in$

$c_{tc} = 2.24\ in$ $\quad c_{tf} = 2.24\ in$

$s_c = 2.34\ in$ $\quad s_f = 3.41\ in$

$\Gamma_{cc} = 16.1\ deg$ $\quad \Gamma_{cf} = 11.173\ deg$

$AR_c = 1.603$ $\quad AR_f = 2.336$

$M := 1.7$

$\beta := \sqrt{M^2 - 1} = 1.375$

$$C'_{N\alpha 1c} := \frac{2 \cdot AR_c \cdot \frac{c_{rc} + c_{tc}}{D_r} \cdot \frac{2 \cdot s_c}{D_r}}{2 + \sqrt{4 + \left(\frac{\beta \cdot AR_c}{\cos(\Gamma_{cc})}\right)^2}} = 2.57$$

$$C'_{N\alpha Tc} := \frac{N_c}{2} \cdot C'_{N\alpha 1c} = 5.14$$

$$C'_{N\alpha 1f} := \frac{2 \cdot AR_f \cdot \frac{c_{rf} + c_{tf}}{D_r} \cdot \frac{2 \cdot s_f}{D_r}}{2 + \sqrt{4 + \left(\frac{AR_f}{\cos(\Gamma_{cf})}\right)^2}} = 5.387$$

$$C'_{N\alpha Tf} := \frac{N_f}{2} \cdot C'_{N\alpha 1f} = 10.773$$

$C'_{N\alpha TBf} := K_{TBf} \cdot C'_{N\alpha Tf} = 13.747$

$C'_{N\alpha TBc} := K_{TBc} \cdot C'_{N\alpha Tc} = 6.975$

$C'_{N\alpha} := C_{N\alpha nc} + C'_{N\alpha TBf} + C'_{N\alpha TBc} = 22.722$

$C'_N := 22.722 \cdot 4\ deg = 1.586$

Figure 9-1 Calculating the pitch normal force for the NASA wind tunnel test model

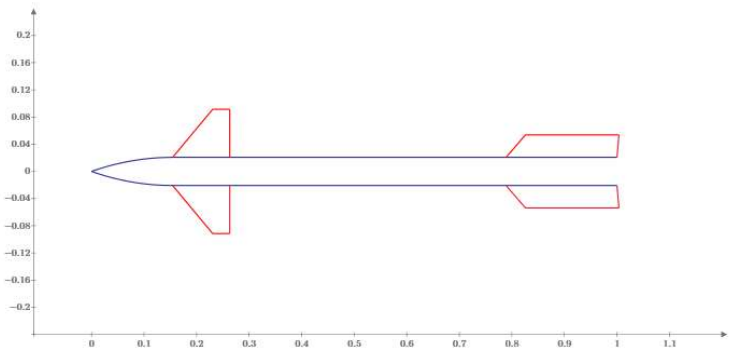

$D_r = 1.67\ in$

$c_{rc} = 4.38\ in$ $\quad c_{rf} = 8.5\ in$

$c_{tc} = 1.31\ in$ $\quad c_{tf} = 7.17\ in$

$s_c = 2.85\ in$ $\quad s_f = 1.33\ in$

$\Gamma_{cc} = 28.304\ deg$ $\quad \Gamma_{cf} = 31.513\ deg$

$AR_c = 2.003$ $\quad AR_f = 0.34$

$M := 1.7$

$\beta := \sqrt{M^2 - 1} = 1.375$

$$C'_{N\alpha 1c} := \frac{2 \cdot AR_c \cdot \frac{c_{rc} + c_{tc}}{D_r} \cdot \frac{2 \cdot s_c}{D_r}}{2 + \sqrt{4 + \left(\frac{\beta \cdot AR_c}{\cos(\Gamma_{cc})}\right)^2}} = 8.156$$

$C'_{N\alpha Tzc} := N_c \cdot C'_{N\alpha 1c} = 32.626$

$C'_{N\alpha TBzc} := K_{TBc} \cdot C'_{N\alpha Tzc} = 40.019$

$C'_{Nz} := 22.722 \cdot 5\ deg = 1.983$

Figure 9-2 Calculating the roll normal force for the NASA wind tunnel test model

10 Appendix 4 - Tools, Equipment, Facilities, & Budget

Software

- Mathcad was the main tool used on this project for modeling, numerical analysis, symbolic analyses, measurement data analysis, and data graphing.
- RockSim was used to validate the parameters calculated by the model such as moment of inertia and center of pressure.
- Microsoft Office Word was used to write this paper
- MathType embedded app for Office was used to create the equations in MS Word
- TurboCAD was used to create most of the figures other than graphs and create the test rocket vertical orientation control system mechanical design

Hardware

- The VTS-1 test rocket was used to validate the pitch and roll aerodynamic parameters

Facilities

- All computer work was done in the author's home office
- Test rocket VTS-1 was built in the author's home woodworking and miscellaneous projects shop including all 3D printing and control electronics assembly
- All test flights were done at Tripoli Central California's launch site at the Maddox Dairy in Helm California

Project Expenses

	Price	Unit	Used	Cost
VOS Unit				
MD89MW-CAN servo	$ 120.00	1	4	$ 480.00
Servo Hubs	$ 9.69	5	4	$ 7.75
LiPo Battery	$ 23.00	2	1	$ 11.50
SAMD21 Arduino	$ 25.00	1	1	$ 25.00
LSM9DS1 IMU	$ 18.00	1	1	$ 18.00
MPL3115A2 Pressure Sensor	$ 16.75	1	1	$ 16.75
Micro SD Holder	$ 6.00	1	1	$ 6.00
MPC2515 CAN Bus module	$ 10.59	2	1	$ 5.30
AP63357 Buck Regulator	$ 5.95	1	1	$ 5.95
Proto Board	$ 12.29	5	2	$ 4.92
Micro SD card	$ 13.68	2	1	$ 6.84
PLA+	$ 40.00	1	0.5	$ 20.00
Misc hardware	$ 20.00	1	1	$ 20.00
Switch	$ 6.00	1	1	$ 6.00
Total				**$ 634.00**
VTS-1 Rocket				
2" tube	$ 21.29	36	6	$ 3.55
3" tube	$ 25.79	36	42	$ 30.09
1.5" tube	$ 28.04	36	14	$ 10.90
3" Coupler	$ 29.16	36	12	$ 9.72
Fin Stock	$ 42.00	1152	288	$ 10.50
Fiberglass cloth	$ 200.00	31	2	$ 12.90
Shock Cords	$ 1.71	1	30	$ 51.30
Misc Hardware	$ 20.00	1	1	$ 20.00
Motor Retainer	$ 25.00	1	1	$ 25.00
Altus Metrum Easy Mini	$ 80.00	1	2	$ 160.00
Total				**$ 333.96**
Motors				
AT I211W motors	$ 73.00	1	7	$ 511.00
AT J350W or AT420R	$ 96.00	1	8	$ 768.00
e-matches	$ 66.00	80	30	$ 24.75
Total				**$ 1,303.75**
Project Total				**$ 2,271.72**

11 Key Variables

A_f	area of the fin
A_r	cross-sectional area of the rocket
AR	aspect ratio of the fins (full span of 2 fins – this comes from wing span)
c_b	sweep length of the fin
c_{MA}	mean chord line
c_r	length of the root chord of the fin
c_t	length of the tip chord of the fin
C_D	drag coefficient
$C_{L\alpha}$	lift coefficient derivative
$C_{N\alpha}$	normal force coefficient derivative
$C_{N\alpha 1}$	normal force coefficient derivative for one fin
$C_{N\alpha T}$	pitch normal force coefficient derivative for N fins
$C_{N\alpha R}$	radial or roll force coefficient derivative for N fins
C_{NTV}	downwash normal force coefficient
$C_{N\alpha TV}$	downwash normal force coefficient derivative
CA_R	radial center of area of the fin
CM_R	radius of gyration – used in the calculation of the roll damping moment
CP	center of pressure
CG	center of gravity
F_D	the drag force
F_L	the lift force
F_N	the normal force
F_{N1}	forcing normal force
F_{N2}	damping normal force
k_{TB}	tail-body interference factor due to the rotation angle of the fin
K_{TB}	tail-body interference factor due to body angle-of-attack
k_{TBCAR}	radial center of pressure interference factor
K_{TBCP}	longitudinal center of pressure interference factor

ℓ	mid chord length
L_{CP}	distance from the tip of the nosecone to the center of pressure
L_{CG}	distance from the tip of the nosecone to the center of gravity
M_{1y}	rotational forcing moment
M_{2y}	rotational damping moment
r	distance from the longitudinal center line of the rocket to a radial location on the fin
r_t	radius of the body tube at the tail section of the rocket
s	span of a fin or canard
v_T	total airstream velocity
x, y, z	axes in the rocket frame of reference – when used as a subscript, the component of that variable aligned with that axis
X, Y, Z	axes in the inertial ground-based frame of reference – when used as a subscript, the component of that variable aligned with that axis
α_{at}	angle-of-attack between the total oncoming airstream and the z-axis (body) of the rocket
α_{ate}	total pitch angle-of-attack including the body angle-of-attack, fin rotation angle, pitch rate induced angle-of-attack, and all tail-body interference factors
α_{ats}	total roll angle-of-attack including the fin rotation angle, roll rate induced angle-of-attack, and all tail-body interference factors
α_f	rotation angle of the fin
α_c	rotation angle of the canard
α_T	angle from the Z-axis opposite the direction of the total oncoming airstream
α	the angle indicating the total rotation about a rocket frame of reference axis, denoted by the axis x,y,z subscript. In the 2-D model, this is also the angle of the rocket's z-axis measured from the Inertial Z-axis as the y-axis remains aligned with the Y-axis
Γ_{sweep}	angle of the leading edge of the fin
Γ_c	angle of the mid chord centerline of the fin
λ	ratio of the fin tip length to the root length
Θ	3-D polar coordinate angle from vertical in 3-dimensional space
τ	ratio of the span of the fin plus body tube to the radius of the body tube
ω	rate of rotation of the rocket axis frame about the x, y, or z-axis, denoted with the axis x,y,z subscript

12 References

Allen, H., & Perkins, E. (1951). *Characteristics of Flow Over Inclined Bodies of Revolution - RM A50L07.* NACA.

Barrowman, J. (1968). *TIR-33 Calculating the Center of Pressure of a Model Rocket.* Centuri Engineering Company.

Barrowman, J. S. (1967). *The Practical Calculation of the Aerodynamic Characteristics of Slender Finned Vehicles, Master's Thesis.* Washington, D.C.: The Catholic University of America.

Barrowman, J. S., & Barrowman, J. A. (1966). *The Theoretical Prediction of Center of Pressure, NARAM-8.* National Association of Rocketry.

Beskin, L. (1946). *Determination of Upwash Around a Body of Revolution at Supersonic Velocities.* Silver Spring, MD: Applied Physics Laboratory, The Johns Hopkins University.

Blair, A. B. (1978). Wind_Tunnel Investigation at Supersonid Speeds of a Canard-Controlled Missile With Fixed and Free-Rolling Tail Fins. *NASA Technical Paper 1316*.

Blair, A. B., Dillon, J. L., & Watson, C. B. (September-October 1993). Experiomental Study of Tail-Span Effects on a Canard-Controlled Missile. *Journal of Spacecrafr and Rockets*, 635-640.

Blair, A. J., Allen, J. M., & Hernandez, G. (June 1983). *Effect of Tail-Fin Span on Stability and Control Characteristics of a Canard-Controlled Missile at Supersonic Mach Numbers.* NASA Technical Paper 2157.

Diederich, F. W. (1951). *A Plan-Form Parameter for Correlating Certain Aerodynamic Characteristics of Swept Wings.* Springfield, VA: NACA TN 2335.

Fetter, T. (2025). *Vertical Trajectory System (VTS) Project*. Retrieved from Speedmotion Rockets: Speedmotionrockets.com

Jarvis, J. (2023, Jan 28). *Development of a Canard-Based Orientation System for High-Power Rockets*. Retrieved from From NAR YouTube Channel: https://www.youtube.com/watch?v=00kFDRk2Cwg&t=12s

Mandell, G. K., Caporaso, G. J., & Bengen, W. P. (1973). *Topics in Advanced Model Rocketry.* Cambridge: MIT Press.

Mayo, E. E. (1967). *Equations for Determining the Effects of Fin Dihedral on Vehicle Stability.* NASA - Memo.

McCormick, B. W. (1995). *Aerodynamics Aeronautics and Flight Mechanics.* New York: John Wiley & Sons, Inc.

Nielsen, J. N. (1988). *Missile Aerodynamics.* Mountain View, CA: Neilsen Engineering & Research.

Pitts, W. C., Neilsen, J. N., & Kaattari, G. E. (1957). *Lift and Center of Pressure of Wing-Body-Tail Combinations at Subsonic, Transonic, and Supersonic Speeds.* NACA Report 1307.

Radius of gyration. (2025). Retrieved from Wikipedia: https://en.wikipedia.org/wiki/Radius_of_gyration

Rocket Rotations. (2023). Retrieved from NASA GlennResearch Center: https://www1.grc.nasa.gov/beginners-guide-to-aeronautics/rocket-rotations/#controlling-the-attitude

Spreiter, J. R. (1950). *The Aerodynamic Forces of Slender Plane and Cruciform-Wing and Body Combinations.* NACA Report 962.